Running Head: STRATIGRAPHIC EVOLUTION OF ONLAP

Title: THE STRATIGRAPHIC EVOLUTION OF ONLAP IN CLASTIC DEEP-WATER SYSTEMS: AUTOGENIC MODULATION OF ALLOGENIC SIGNALS

Authors: EUAN L. SOUTTER[1*], IAN A. KANE[1], ARNE FUHRMANN[1], ZOË A. CUMBERPATCH[1] and MADS HUUSE[1]

Institutions:

[1]School of Earth and Environmental Sciences, University of Manchester, Oxford Road, Manchester M13 9PL, UK

Email: euan.soutter@manchester.ac.uk

Keywords: Deep-water, confined basin, onlap, autogenic, Grès d'Annot

ABSTRACT

Seafloor topography affects the sediment gravity flows that interact with it. Understanding this interaction is critical for accurate predictions of sediment distribution and paleogeographic or structural reconstructions of deep-water basins. The effects of seafloor topography can be seen from the bed-scale, through facies transitions toward intra-basinal slopes, to the basin-scale, where onlap patterns reveal the spatial evolution of deep-water systems. Basin margin onlap patterns are typically attributed to variations in subsidence or sediment supply, with few studies emphasising the importance of predictable spatio-temporal autocyclic flow evolution. This study documents onlap styles within the confined Eocene-to-Oligocene deep-marine Annot Basin of SE France. Measured sections, coupled with architectural observations, mapping and paleogeographical interpretations, are used to categorize onlap termination styles and place them within a generic stratigraphic model. These observations are compared with a simple numerical model. The integrated stratigraphic model predicts that during progradation of a deep-water system into a confined basin successive onlap terminations will be partially controlled by the effect of increasing flow concentration. Initially thin-bedded low-density turbidites of the distal lobe fringe are deposited and drape basinal topography. As the system progrades these beds are overlain by hybrid beds and other deposits of higher-concentration flows developed in the proximal lobe fringe. This transition is therefore marked by intra-formational onlap against the underlying and lower-concentration lobe fringe that drapes the topography. Continued progradation results in deposition of lower-concentration deposits within the lobe off-axis, resulting in either further intra-formational onlap against the lobe fringe, or onlap directly against the hemipelagic basin margin. Basinal relief is gradually reduced as axial and higher volumes flows become more prevalent during progradation, causing the basin to become a bypass zone for sediment routed down-dip towards the next sub-basin. This study presents an autogenic mechanism for generating complex onlap trends without the need to invoke allogenic processes. This has implications for sequence stratigraphic interpretation, basin subsidence history, reservoir prediction and forward modeling of confined deep-water basins.

INTRODUCTION

Deep water lobes are amongst the largest sedimentary bodies on Earth and comprise terrigenous sediment shed from the adjacent continental shelf and slope (e.g., Piper et al., 1999; Talling et al., 2007; Prélat et al., 2010; Clare et al., 2014). They offer a record of Earth's climate and sediment transport history, and form valuable hydrocarbon reservoirs, aquifers and sites of mineral accumulation (e.g., Weimer and Link, 1999; Hodgson et al., 2009; Sømme et al., 2011; Bell et al., 2018). Sediment-gravity-flow evolution across unconfined deep-water settings results in a fairly uniform radial spreading and deceleration of flows and development of elongate to lobate sedimentary bodies with predictable facies transitions (e.g., Baas et al. 2004; Hodgson et al., 2009; Spychala et al., 2017).

Sediment-gravity-flows encountering seafloor topography in confined basin settings form a range of onlap geometries often associated with complicated sedimentary facies (Fig. 1) (e.g., Kneller, 1991; Haughton, 1994; Wynn et al. 2000; McCaffrey and Kneller, 2001; Smith, 2004; Amy et al., 2004; Gervais et al. 2004; Smith and Joseph, 2004; PuigdefàBregas et al., 2004; Gardiner, 2006; Mayall et al. 2010; Tinterri et al. 2016; Hansen et al. 2019). The effect of seafloor topography on sediment gravity flows, their deposits, and onlap styles has been studied through outcrop (e.g., Kneller et al. 1991; Sinclair et al., 1994; Bakke et al., 2013) and subsurface data (e.g., Prather et al., 1998; 2012; Covault and Romans, 2009; Bakke et al., 2013), and numerical (e.g., Smith, 2004; Kubo, 2004; Gardiner, 2006; Sylvester et al., 2015) and physical models (e.g., Kneller, 1995; Kneller and McCaffrey; 1995; Amy et al., 2004; Brunt et al., 2004; Kubo, 2004). Seafloor topography is generated by a variety of geological processes, such as: pre-depositional tectonic deformation (e.g. Jackson et al. 2008; Kilhams et al. 2012) syn-depositional tectonic deformation (e.g. Davies et al., 1992; Haughton, 2000; Grecula et al., 2003; Tomasso and Sinclair, 2004; Kane et al. 2010; Salles et al., 2014), mass transport deposit relief (e.g. Armitage et al., 2009; Ortiz-Karpf et al., 2015; 2016; Kneller et al., 2016; Soutter et al., 2018) and salt diapirism (e.g. Hodgson et al., 1992; Kane et al. 2012; Prather et al. 2012; Oluboyo et al. 2014; Doughty-Jones et al., 2017). Improved prediction of sediment-gravity-flow deposit distribution around seafloor topography is therefore critical for both paleogeographic reconstructions (e.g., Pinter et al., 2017) and stratigraphic hydrocarbon trap risking (e.g., McCaffrey and Kneller, 2001).

The onlap geometry (3D shape of the event bed or sequence of event beds at pinch-out) and facies (internal sedimentary characteristics of the event bed at pinch-out) (Fig. 1A), herein termed onlap termination, are controlled by: 1) flow magnitude, duration, velocity, thickness, concentration, sediment composition; 2) the gradient and incidence angle of the counter slope; and 3) seafloor composition and induration. Typically, high concentration flows and steep counter slopes cause abrupt terminations, whereas low concentration flows and shallow counter slopes cause draped terminations (Fig. 1) (Smith and Joseph, 2004; Bakke et al. 2013). Flows with a high mud content may also be more prone to varying degrees of rheological transformation approaching counter slopes, resulting in complicated facies distributions at confining basin margins (Fig. 1) (Barker et al., 2008; Patacci et al., 2014; Southern et al., 2015).

Recent field-based studies on the spatial and temporal evolution of unconfined submarine lobes have used the longitudinal evolution of flows and their associated facies to establish criteria for differentiating lobe sub-environments at the bed-scale (e.g., Prélat et al. 2009; Grundvag et al. 2014; Spychala et al. 2017). The applicability of these facies associations to highly confined lobe or 'sheet' systems and the complex system-scale stacking patterns that they may produce is only recently being investigated (e.g. Marini et al. 2015; Spychala et al. 2015, 2017; Bell et al. 2018; Dorrell et al. 2018; Fonnesu et al. 2018; Liu et al. 2018). Previous flow-dependant onlap models mainly focussed on end-member geometries (e.g. McCaffrey and Kneller, 2001; Smith, 2004; Smith and Joseph, 2004). As yet

there is no generic model to account for the wide variety of longitudinal flow evolution and their manifestation at onlap surfaces through the fill of a confined basin.

This study uses the well-constrained Cenozoic Annot Basin of SE France to integrate bed-scale and basin-scale onlap observations into a generically applicable depositional model. The aims of this study are to: i) reappraise the Annot Basin stratigraphy with respect to specific deep-water sub-environments, with particular emphasis on the poorly-studied eastern margin of the basin, ii) document lateral facies changes within beds approaching the basin margin and relate these facies changes to longitudinal flow evolution, iii) assess how the longitudinal evolution of confined flows impacts onlap geometry and stacking patterns, and iv) integrate these observations into a generic model for the evolution of onlap within deep-water basins.

THE ANNOT BASIN

Basin Structure

The 160 km long and 80 km wide (Clark and Stanbrook, 2001) Cenozoic foreland basin of the western Alps formed due to SW-directed collision of the Adria and European plates, and subsequent loading of the European plate by the Alpine orogenic wedge (Fig. 2; Fig. 3) (e.g. Ford et al., 1999). This orogenic deformation is represented in the foreland basin stratigraphy by a progressive younging to the south-west (e.g. Ford et al., 1999; Du Fornel et al. 2004). Sediment deposition within the basin was affected by complicated basinal topography (e.g. Joseph and Lomas, 2004), which formed due to Late Cretaceous northward-directed Pyrenean compression which was subsequently overprinted by Cenozoic SW-directed Alpine compression (Fig. 3) (e.g. Apps et al., 2004). This resulted in NW-SE orientated synclinal sub-basins with E-W anticlinal sills. The synclines are interpreted as the surface expression of underlying Alpine thrust fault propagation folds (Fig. 3) (e.g. Elliott et al. 1985; Apps, 1987; Ravenne et al. 1987).

The Annot sub-basin, herein termed the Annot Basin, is one of the exhumed synclinal Cenozoic depocenters within the Alpine foreland basin, representing the proximal end of the deep-marine Annot – Grand Coyer – Chalufy chain of 'sub-basins' (Fig. 2; Fig. 3) (e.g. Du Fornel et al., 2004). The Annot Basin is bounded to the south by the SW-NE Rouaine Fault Zone, which acted as an entry point for sediment gravity flows into the basin (e.g. Salles et al. 2014) (Fig. 2; Fig. 3; Fig. 5). The SW-NE Braux normal fault is related to this fault zone and created local bathymetric relief during the Late Eocene (e.g. Tomasso and Sinclair, 2004) (Fig. 3; 4). The western and eastern margins of the basin are defined by fault-propagation anticlines created by Mesozoic blind-thrusts (Fig. 3; 4) (e.g., Apps, 1987). The eastern margin is formed by the Melina anticline, or 'kink zone' (Apps, 1987), and the western margin by the Puy du Rent anticline (Fig. 3; 4B). These anticlines were developing during deposition of the Annot turbidites, causing syn-depositional rotation of the basin depocenter towards the west (Fig. 3) (e.g Salles et al., 2014).

E-W orientated Pyreno-Provincale structures also affect the Annot Basin structure, with the northern extent of the basin formed by the Aurent anticline (Fig. 3). This structure forms a gently southward-dipping terminal slope (e.g., McCaffrey and Kneller, 2004). More minor basin-floor relief may have been formed by the E-W Fugeret anticline, which lies between the Rouiane fault zone and the Aurent anticline (Fig. 3) (Salles et al., 2014).

Stratigraphic Evolution

The Annot Basin has the same transgressive Cenozoic foreland basin stratigraphy as is seen across the western Alps (Fig. 2; Fig. 3) (e.g. Sinclair, 1997), with Oligocene shallow-marine limestones of the Calcaires Nummulitique overlain by deep-marine marls of the Marnes Bleues. The Marnes Bleues records the deepening of the basin, with foraminifera suggesting water depths of ~100 m at the base of the succession, to ~800 m by the end of deposition (Mougin, 1978). Siliciclastic sediment supply began abruptly in the Late Eocene (35.2 Ma) as the Corsica-Sardinia massifs were uplifted via subduction-related back-thrusting towards to the south (Fig. 2) (e.g. Stanley and Mutti, 1980; Apps, 1987). This resulted in a depositional shift from the marls of the underlying Marnes Bleues, into south-to-north dispersing clastic sediment gravity flows of the Grès d'Annot. An upwards coarsening trend within the Grès d'Annot suggests progradation of the clastic system, most-likely related to fan delta advance (Fig. 3) (e.g., PuigdefàBregas, 2004).

During early clastic deposition the Annot Basin was located on the western-side of a distal submarine fan extending over the foreland basin, with flows entering the basin from syncline-bound fan-deltas to the south (Fig. 2) (e.g., Stanley, 1980; Sinclair, 2000; Joseph and Lomas, 2004) and being dispersed northwards through relay ramps within the Rouaine Fault Zone (Fig. 3; Fig. 6) (Joseph and Lomas, 2004; Salles et al., 2014). This early deposition is represented in the Annot Basin by low-density turbidites, often referred to as the Marnes Brunes Inferiérures (e.g., Stanbrook and Clark, 2004), which form the distal equivalent of the Grès d'Annot. The lowermost Grès d'Annot member, termed Le Ray (Puigdefabregas, 2004) or the A Member (Du Fornel, 2004), onlaps both the underlying Marnes Brunes and Marnes Bleues slope (Fig. 3; 5). Early flows were confined by the Braux Fault to the west, a combination of the Braux Fault and the Fugeret anticline to the north, and by the Melina anticline to the north-east (Salles et al., 2014). The sediment entry point shifted throughout deposition of the Grès d'Annot, with a more easterly Late Eocene entry point suggested for these early flows, as evidenced by an up-stratigraphy rotation of paleocurrents from NE- to NW-directed (McCaffrey and Kneller, 2004; Salles et al., 2014). Alternatively, this may be an apparent repositioning of the sediment entry point as the basin depocenter itself migrated gradually westward due to Alpine compression (Salles et al., 2011; 2014). The remaining Grès d'Annot members were confined by the major Melina (east), Puy du Rent (west) and Aurent anticlines (north) as the topography of the Braux Fault and Fugeret Anticline was healed relatively early in the Oligocene (Fig. 3) (Salles et al., 2014).

The basin gradually filled throughout the early Oligocene, with contemporaneous deposition occurring in the parallel Grand Coyer sub-basin to the north-east (Salles et al., 2014). Once the basin was largely filled, the Aurent Anticline ceased to terminally confine flows, and flows bypassed the Annot Basin into the Grand Coyer and Chalufy sub-basins (Fig. 2) (e.g., Apps, 2004; Salles et al., 2014). Few channel-fills are seen within the Grès d'Annot succession, and the depositional architecture is interpreted as being predominantly sheet-like (Apps, 1987).

DATA AND METHODS

The dataset comprises 50 (581 m cumulatively) sedimentary logs collected along sections oblique to depositional-dip along the eastern margin of the Annot Basin (Fig. 4; 5; 6). Logs were collected at 1:10 scale and individual beds were walked out at outcrop (Fig. 6). Higher resolution 1:2 scale logs were collected from some beds approaching onlap. Logs within thin-bedded facies were collected at a 1:5 scale to allow accurate representation of their thicknesses and structures. Samples of individual facies and individual beds were collected in order to quantitatively constrain lateral grain-size and matrix changes. 96 3D paleocurrent measurements were collected (Fig. 5), with 2D paleocurrent measurements qualitatively noted.

Margin Correlation

Sedimentological contacts between the discrete members of the Grès d'Annot from the geological maps of PuigdefàBregas et al. (2004), Du Fornel et al. (2004) and Salles et al. (2014) were ground-truthed and compared to observations made by this study (Fig. 3). The observations of stratigraphic contacts made during this study most closely agree with those made by PuigdefàBregas et al. (2004), therefore their geological map was used for placement of sedimentary logs within members and for the intra-member correlation of sedimentary logs (Fig. 5; 6). This allows facies transitions across the basin to be assessed both spatially and temporally. Where member boundaries are unclear due to the resolution of the geological map the top of individual members is defined by either abrupt facies changes, commonly an abrupt coarsening and thickening of event-beds (Fig. 9), or lateral relationships and correlations (Fig. 5). The nomenclature used by PuigdefàBregas et al. (2004) and Salles et al. (2014) are reconciled to enable comparisons to be made between the two (Fig. 3).

Detailed correlations of the Le Ray member are based on the identification of key surfaces, such as onlap surfaces, and walking out of individual beds (Fig. 6). Where beds could not be walked out units were correlated based on the methodology of Prélat et al. (2009) for the identification of the hierarchical elements that builds lobes e.g. beds, lobe elements and lobes.

FACIES ASSOCIATIONS

Facies associations (FA) have been interpreted based on the dominant lithofacies (LF) and depositional features of a given succession (Table 1). The dominant lithofacies has been described and interpreted within each facies association in order to justify their placement within that sub-environment. The lobe sub-environments of Spychala et al. (2017) are used as they best fit the observations made in this study (Fig. 8A). The onlap geometry of each lithofacies, and therefore the inferred onlap geometry of the facies association in which that lithofacies dominantly occurs, is summarized in Figure 7. Facies associations are presented from proximal to distal positions on the lobe in the following section.

FA 1 Lobe-axis

Observations.--- Facies association 1 is dominantly composed of one lithofacies: thick-bedded (0.5 – 2 m) sandstones (LF 1A) (Fig. 10A, B, E), with thin-bedded (0.01 m – 0.5 m) sandstones (LF 1B) and medium-bedded sandstones (0.1 – 0.8 m) (LF 3) commonly associated. LF 1B is composed of medium- to cobble-grade (most typically coarse-grained), poorly-sorted, massive sandstones (Fig. 10B) and is less prevalent than LF 1A. Individual beds have erosive bases, often with groove, flute and tool marks, and irregular tops. Beds are often lenticular, thickening and thinning from <10 cm before pinching out over tens of metres. The beds often occur within successions of medium-bedded sandstones (LF 2) below packages of LF 1.

The thick-bedded LF 1A sandstones are medium-grained to granular sandstones with bed bases that are flat (at exposure scale) or erosive (Fig. 8; 10; 12B). Flat bases are most prominent when overlying mudstones, while erosive bases are most commonly expressed as amalgamation surfaces (Fig. 9B, C, D). Both bedding-parallel and erosive bases are associated with decimeters of deformation in the underlying beds. This deformation obscures the primary depositional characteristics of the underlying beds, making interpretation of the deformed beds difficult. Bed bases with steeper dips than the bed top are observed at pinch-out of these beds (Fig. 11B), with bed bases steepening towards the pinch-out. Amalgamation surfaces are identified by mudstone-clast-rich rugose horizons, abrupt grain-size breaks and truncated trace fossil burrows. Bed tops are flat and exhibit little depositional relief. Beds are typically structureless, with rarely preserved faint parallel lamination and tractional structures, and ungraded, though some beds show weak normal grading (Fig. 9B, C, D).

Interpretations.--- The presence of erosive bed bases with tool and grooves indicates that LF 1A beds were deposited by high concentration flows that initially carried large clasts and other detritus at the base of the flow. Superimposed flute marks, normal grading and tractional structures are indicative of evolution to a less concentrated more turbulent flow. The rarity of tractional structures and commonly massive and poorly sorted beds, however, indicates that these beds were deposited rapidly (*sensu* Lowe, 1982). This is most likely due to a reduction in flow capacity (*sensu* Hiscott, 1994), preventing the formation of grading and the preservation of bedforms. These turbidites are therefore interpreted as

high-density turbidites (*sensu* Lowe, 1982). The presence of deformation structures beneath these flows has been attributed to high shear stresses acting on the seabed (e.g. Clark and Stanbrook, 2001; PuigdefàBregas et al. 2004). These laterally extensive (up to 1 km where outcrop allows) high-density turbidites, which are commonly amalgamated, are interpreted to be analogous to lobe axis deposits observed elsewhere (e.g., Prélat et al. 2009).

The coarse grain size and thin-bedded nature of LF 1B suggests that these beds were deposited as a coarse-grained lag in a bypass-dominated part of the system. The lenticular geometry suggests that either i) flow energy, and therefore bypass potential, was not homogenous laterally within the flow or ii) erosion by subsequent flows, or by waxing of the flow through time (Kane et al., 2009), scoured the bed top (Fig. 10B). Because this lithofacies is confined stratigraphically to sequences underlying thick-bedded and amalgamated sandstones of similar grain sizes they are inferred to be laterally related. These lags are interpreted to represent a mostly bypassing equivalent of the thick-bedded sandstones within the lobe axis.

FA 2: Lobe off-axis

Observations.--- Facies association 2 is primarily composed of normally-graded medium-bedded (0.1 – 0.8 m) fine- to medium-grained sandstones (LF 2) with flat to slightly erosive bed bases, and flat bed-tops (Fig. 7; 11A). Flutes and grooves are often seen at bed bases. Ripples at bed tops commonly show opposing paleoflow directions to those measured from flutes and grooves on individual event beds (Fig. 4). Beds pinch-out abruptly towards the basin margin, and can often be traced away from the onlap surface to a parent thick-bedded sandstone (Fig. 7). In the uppermost stratigraphy of the basin LF 2 commonly has highly irregular bed tops with abundant tractional structures, such as climbing ripples and convolute lamination (Fig. 10E). These beds are termed LF 2B.

Interpretations.--- The presence of flutes, normal grading and tractional structures indicate that the LF 2 beds were deposited by waning, turbulent flows which were able to rework the aggrading deposit (Bouma, 1962). This suggests that these flows were more dilute than the parent flows of the thick-bedded sandstones (LF 1). These medium-bedded sandstones are therefore interpreted as medium-density turbidites and are differentiated from low-density turbidites by bed thicknesses being greater than 10 cm and a coarser grain size. These medium-density turbidites also have a thicker massive interval at their base compared to low-density turbidites. Opposing paleocurrent directions within event beds is characteristic of flows encountering topography (e.g., Kneller et al., 1991), indicating many of these beds were deposited in close proximity to a basin margin. Coarser, denser parts of the flow may be more strongly influenced by topography than the upper more dilute part of the same flow (Bakke et al., 2013).

The finer, better sorted and thinner-bedded nature of this lithofacies compared to thick-bedded sandstones indicates that these beds were deposited beyond the axis of the lobe (off-axis) (Prélat et al. 2009; Bell et al., 2018) (Fig. 8). LF 2B is interpreted as representing flows that deposited close to the basin

margin or possibly within slump scars on the basin margin. Bypassing flows deflected by the margin or trapped within the scars, caused complicated oscillatory flow patterns to develop which deformed the aggrading deposits (Pickering and Hiscott, 1985; Tinterri et al. 2016; Cunha et al. 2017). An example of this can be seen at Tête de Ruch, where this facies dominates a ~10 m scar fill (PuigdefàBregas et al. 2004) and is overlain by thin-beds showing simple uniformly directed ripples and plane-parallel lamination (Fig. 5; 12C). These thin beds were deposited over the scar-fill where flows were relatively unconfined, allowing more uniform and waning flow deposition to dominate.

FA 3: Proximal fringe

Observations.--- Facies association 3 is dominated by medium- to thick- bedded (0.1 m – 1.2 m) bi- or tri-partite event beds (LF 3) (Fig. 9; 11C; D). These beds are composed of a lower division of medium- to thick-bedded sandstone (LF 1 and LF 2) with an irregular top which is loaded and/or eroded into by an overlying argillaceous sandstone (Fig. 10D). The middle division is an argillaceous sandstone, poorly-sorted and often deformed, which appears as a sheared fabric (Fig. 10D). The argillaceous sandstone can either contain clasts of the underlying sandstone or be clast-poor. Organic matter (< 70 cm in length) may be present within this bed, with organic-rich sandstones typically thicker than the more argillaceous sandstones. Elongate organic matter is usually aligned with its long-axis approximately parallel to paleoflow recorded on the bed base (Fig. 10C).

Argillaceous sandstones, which are rich in cleaner sandstone clasts, commonly occur where the lower, cleaner sandstone is coarser-grained, thus most sandstone clasts seen tend be coarse-grained than the argillaceous matrix. This deposit can show variable sand-to-mud ratios. Higher sand contents within this middle division are associated with increased prevalence of lamination, with cm-scale banding (mud-concentrated laminae) sometimes evident, and higher mud contents associated with more sheared and poorly-sorted deposits. Both of these divisions may contain coarse-sandstone to granule-sized quartz grains supported within the matrix.

Overlying this argillaceous sandstone, medium-bedded, often muddy sandstone may occur, although it is sometimes difficult to assess whether this sandstone is part of the underlying event-bed or represents a separate event-bed (Fig.11D). This sandstone has an irregular base and can show loading and foundering into the underlying argillaceous sandstone (Fig. 10D). The bed top is typically flat or mounded. Approaching basin margins these beds can be seen to transition laterally from thick-bedded sandstones (Fig. 14A, B).

The middle division of the bed may pinch out before the underlying and overlying sandstones, which then amalgamate at the onlap surface (Fig. 14C), forming a complicated and often muddy pinch-out (Fig. 15). Stratigraphically this lithofacies dominantly occurs following the thin-bedded dominated sequence and underlying the medium- to thick-bedded sandstones (Fig. 9).

Interpretations.--- The basal and upper sandstones within these bi- or tripartite event beds are interpreted as either high- or medium-density turbidites. The massive, poorly sorted, and mud-rich composition of the division encased by these turbidites is interpreted as being caused by en-masse deposition of a laminar and cohesive flow (e.g., Middleton and Hampton, 1973; Mulder and Alexander, 2001). This bed division is therefore interpreted as a debrite. The irregular contact seen between these divisions has been attributed to complex short-wavelength soft-sediment deformation and erosion (e.g. Fonnesu et al. 2015). Where the overlying turbidite is relatively thick it is difficult to differentiate between a debritic or deformed (see LF 1 basal deformation) origin for the middle division, particular when the overlying turbidite has foundered into the underlying division (e.g. Fonnesu et al. 2015). Where the middle sandstone division is slightly cleaner, with lamination and/or banding, the sandstone is interpreted as being deposited by flows transitional between laminar and turbulent and therefore termed a transitional flow deposit (Baas et al., 2011). These tri-partite event beds therefore contain deposits of both turbulent and laminar flow regimes and are subsequently interpreted as hybrid beds (*sensu* Haughton, 2009).

It is suggested that the more organic-rich linked debrites, with decimeter clasts of terrestrial debris, are derived from flows which originated from events in the hinterland that carried significant amounts of terrestrial debris into the marine environment (see also Hodgson, 2009). These beds may therefore represent deposits from particularly high-magnitude flows, which may explain their greater average thickness compared with the more argillaceous hybrid-beds. It is also possible that the organic material was staged for significant periods of time on the shelf, making terrestrial debris a poor indicator of flow magnitude. The close association of terrestrial debris and coarse grain-sizes in these relatively distal environments, however, indicates that these beds were the result of high magnitude or 'outsize' flows that were capable of significant substrate erosion (Fonnesu et al. 2018). Incorporation and disaggregation of this eroded substrate will have primed these flows for rheological transformation (Kane et al. 2017; Fonnesu et al. 2018). LF 1 can be seen to transform into these hybrid beds over tens of meters approaching the slope, further indicating that these beds were highly erosive and prone to rheological transformation, even within proximal positions, due to forced deceleration against the basin margin (e.g. Patacci et al. 2014). The presence of high-amounts of erodible and muddy draping substrate on the basin margin will aid in short length-scale flow transformation within these high-magnitude flows (Fig. 15) (e.g. Fonnesu et al. 2018).

It may also be possible that the debritic division of these beds represents high-concentration turbidity currents hitting the counter-slope, causing intra-basinal slope instability and failure. The turbidity current will then have aggraded around this failure, represented depositionally by a 'sandwiched' debrite (e.g. McCaffrey and Kneller, 2001). It is difficult to differentiate between a flow transformation or slope failure origin for the co-genetic debrite at outcrop, however the presence of large organic clasts within an identified debritic division may favor a flow transformation origin.

Because these beds dominantly underlie the thicker-bedded and more sandy turbidites of FA 1 and 2 they are interpreted as being depositionally adjacent (*sensu* Walther, 1894) (Fig. 8). An abundance of hybrid beds indicates a more distal lobe sub-environment compared with the axis and off-axis deposits of FA 1 and FA 2 (e.g., Hodgson, 2009; Jackson et al. 2009; Kane et al., 2017; Fonnesu et al. 2018). This sub-environment is termed the lobe fringe. FA 3 is therefore interpreted as being analogous to lobe fringe deposition seen in unconfined systems (e.g. Spychala et al. 2017). The lobe fringe can be further subdivided into a lateral and frontal fringe, with the lateral fringe having a lower proportion of hybrid beds compared to the frontal fringe (Spychala et al. 2017). In confined settings this definition is complicated because flow deceleration against lateral slopes cause flow transformations and subsequent enrichment of hybrid-beds within the lateral fringe (Fig. 8A; 17). This relationship is also evident within the Late Cretaceous Britannia Sandstones of the North Sea, where flows underwent rheological transformation against a lateral slope (Lowe and Guy, 2000; Barker et al. 2008). This study thus uses the general term proximal fringe as the frontal and lateral fringe are expected to be similar due to the counter-slope causing a prevalence of hybrid-beds in both settings (Fig. 8; 17).

It should also be noted that particularly erosive flows within the axis and off-axis also generate hybrid-beds at the onlap surface (e.g. Patacci et al. 2014; Fonnesu et al. 2018). This can make lobe-sub-environment interpretation challenging when adjacent to a steep basin margin as much of the succession may be margin-affected over short length-scales (10s m) (Fig. 15) and therefore not represent their primary lobe-scale paleogeographic position (e.g. Southern et al. 2015). This is enhanced in tectonically active basins where flow types can be highly variable (e.g. Mutti et al. 2009). Facies 'back-stripping' may therefore need to be attempted to assess the lobe-scale sub-environment (Fig. 15). These short-length-scale margin-affects and attempts at back-stripping are summarised on Figure 17 and 18.

FA 4: Distal fringe

Observations.--- Facies association 4 is dominated by thin-bedded (0.01 – 0.1 m) siltstones to fine-grained sandstones (LF 4) that form laterally continuous event beds (Fig. 8; 12A; 14). Parallel and convolute lamination is common (Fig. 10F). Beds are normally-graded, with ripples commonly seen at bed tops (Fig. 10F). Ripples may show multiple and opposing paleocurrent directions within single beds. Beds tend to pinch-out over 10s-100s of meters towards the basin margin (Fig. 13), with amalgamation of event-beds sometimes observed towards the onlap surface, causing local bed thickness increases within a regional thinning trend. Slumping and folding of beds (LF 5) is evident within this FA, particularly immediately underlying the abrupt transition to dominantly medium- and thick-bedded sandstone sequences (Fig. 9A; Fig. 10G). Fold axis measurements indicate deformation was both oblique and perpendicular to paleo-slopes. Stratigraphically, these beds immediately overlie the Marnes Bleues, forming a distinct sequence that significantly drapes the Marnes Bleues slope (Table 1). This lithofacies becomes less common up stratigraphy (Fig. 9).

Interpretations.--- The fine grain-size, abundance of tractional structures, and dominance of thin-beds within LF 4 indicates deposition from dilute, low-density turbidity currents (*sensu* Lowe, 1982). The narrow grain size range (dominantly silt) of these slope draping beds is numerically predicted as flows composed of silt or mud show a quadratic decrease in settling velocity and a consequent increase in the likelihood of flow inflation far above the initial flow depth (Dorrell et al. 2018). Because these beds are able to drape the existing relief they are suggested to have healed much of the initial relief present on the Marnes Bleues slopes (Fig. 7; 12A). Pervasive slumping within these successions (LF 5) is interpreted to represent slope failure on the steep basin margins (Fig. 10G). Progressive deformation and seismicity along the Alpine thrust-front is suggested as the primary reason for slope failure (Fig. 2). Failure scars are suggested to contribute to some of the heterogeneity seen within the overlying medium- and thick-bedded sandstones by creating a rugose topography high on the slope (Fig. 15).

The lateral continuity, fine grain-size and thin-bedded character of the thin-beds is consistent with both levee deposition and lobe fringe deposition. Because of the few long-lived channels identified, and the low stratigraphic position of these beds within a prograding lobe they are not interpreted to be levee deposits (Fig. 8), but are instead attributed to the distal fringe of a submarine lobe on the basin floor (e.g. Boulesteix et al. 2019) (Fig. 8), which caused termination of Marnes Bleues carbonate deposition. This is supported by the published paleogeographic position of the lowermost Grès d'Annot (Fig. 2) (Apps et al., 2004; Joseph and Lomas, 2004; Salles et al., 2014). The relative lack of hybrid beds within the LF5 sequence also supports a distal lobe fringe interpretation (Fig. 8; 10A) (Spychala et al., 2017).

STACKING PATTERNS

Le Ray

Confined basins have previously been associated with 'sheet-like' deposition, where incoming flows are entirely confined by the basin margins, resulting in tabular stratigraphy with little or no autogenic compensational stacking (e.g. Sinclair and Tomasso, 2002). Numerical (Dorrell et al. 2018), subsurface (e.g. Beaubouef and Friedmann, 2000), and outcrop studies (e.g. Spychala et al. 2016; Bell et al. 2018; Liu et al. 2018), however, have shown the stacking pattern complexity that may arise within basins that display variable degrees of confinement. This study uses data from the lowermost member of the Grès d'Annot, the Le Ray member (Fig. 5; 6), to build on these studies. Le Ray (PuigdefàBregas et al., 2004), or member A (Du Fornel et al. 2004), was fully confined by the basin margins during its deposition (Callec, 2004; Salles et al. 2014).

Unit 1.--- This unit comprises a sequence of thin-bedded low-density turbidites (LF 4) overlain abruptly by medium and thick-bedded high-density turbidites (LF 1 and 2). These thick-bedded sandstones correlate with a thick-sequence of thin-bedded turbidites about 800 m to the NW adjacent to the Braux Fault footwall (Fig. 3; 6). This transition is either caused by flow over-spill across the

paleobathymetry of the Braux Fault or draping of the lower-density part of the flow up the Braux Fault topography. Correlation of this unit toward the east is hindered by lack of exposure.

Unit 2.--- Proximal Unit 2 is characterized by a thick 33 m amalgamated sandstone body interpreted as being deposited by high-concentration turbidity currents. Indicators of erosion, such as scours and decimetre scale mud-clasts, indicate that this was a region of significant bypass (e.g. Stevenson et al. 2015) and is interpreted to represent the lobe axis through Le Ray deposition. Down-dip this unit has been subdivided into Unit 2A and 2B based on facies and stacking. Unit 2B is composed of thin-bedded turbidites that drape the frontal confinement of the early Annot Basin and stack aggradationally (Fig. 11A). This confinement was caused by a combination of the basin closure due to the NW-SE Melina anticline, the E-W Fuguret anticline and the NE-SW Braux Fault (Fig. 3). Unit 2A represents an abrupt transition into thicker-bedded sandstones that pinch-put against the underlying Unit 2A. These sandstones can be sub-divided into different lobes based on the correlation of intervening packages comprising low-density turbidites (LF 4) overlain by hybrid-beds (LF 3), medium-density turbidites (LF 2) and amalgamated high-density turbidites (LF 1). These lobes represent the depositional products of the bypassing flows from the proximal thick sandstone body, forming the lobe axis.

The axis of each of these lobes steps farther into the basin, suggesting allogenic progradation through increasing sediment flux from the uplifting Corsica-Sardinia hinterland (e.g. Apps et al. 1987). This pattern is not uniform, however, and a degree of compensational stacking is clearly visible, with the axis of successive lobes (represented by amalgamated high-density turbidites) overlying the fringes of underlying lobes, which represented lows on the seafloor (e.g. Deptuck et al. 2008; Prélat et al. 2009). These stacked lobes could also represent lobe 'fingers' that were focussed between the lows of the previous axial deposits (e.g. Groenenberg et al. 2010). In this case the apparent basinward stepping of the Le Ray lobes may be autogenically-driven, as flows are focussed between the lows and build passively into the basin. This explanation may operate in tandem with allogenic progradation, particularly during early deposition, due to the prevalence of these finger-like geometries within the basal stratigraphy of lobe complexes (e.g. Prélat et al. 2009; Groenenberg et al. 2010). These indicators of compensational stacking are at odds with the prevailing suggestions that confined basins can simply be described as sheet-like and fit with the recent work indicating that lobes in confined basins are characterized by more complicated stratigraphic relationships (Bell et al. 2018).

The presence of thick and coarse sandstones in distal positions has also been described in subsurface datasets of submarine lobes and lobe elements and has been attributed to flow-stripping of the upper dilute parts of flows over the basin's confining topography, leaving behind the coarser parts of the flow (e.g. Jobe et al. 2018). This process may also contribute to the preservation of the thick and abruptly terminating sandstones within Unit 2 of the Le Ray member.

Unit 3.--- This unit has been differentiated as it cannot be reliably correlated to another unit. It is possible that Unit 3 represents the distal expression of the upper parts of Unit 2, however the lack of exposure between the proximal and distal parts of the upper Le Ray prevents reliable correlation.

Alternative Interpretations.--- The observed intra-formational onlap against the low-density fringe at the Col du Fa locality is likely caused by the inferred proximity of the basin margin. An alternative explanation for this stratigraphic relationship may be the presence of a large erosional feature, such as a scour, at the Col du Fa margin. Such scours are interpreted higher in the basin stratigraphy at Tête du Ruch (e.g PuigdefàBregas et al. 2004), and show the same intra-formational onlap relationship (Fig. 11B). Decametre-thick scour fills are also suggested to be present in the Grès d'Annot at Peira Cava (Lee et al. 2004). The scour would have created accommodation space to be filled by the incoming flows, resulting in the onlap geometries described by this study. Exposure limits further analysis of this problem, however a scour interpretation is not believed to affect the underlying principles of this study as the low-density turbidites still drape the scour and are onlapped by the later higher-density turbidites.

Another explanation for the observed intra-formational onlap may be that the low-density fringe (Unit 1) was tilted (e.g. Salles et al. 2014) and subsequently onlapped by higher-density flows when the basin was relatively static. Unit 1 may therefore represent the distal extents of early Le Ray (i.e. the Marnes Brunes Inferiérures), while the onlapping Unit 2 is either more proximal and late-stage Le Ray or early La Barre (Fig. 3). Differential compaction between the basin centre and basin margin may have also acted to enhance the tilting effect (Sinclair, 1994). The inability to walk out individual units between outcrop localities again makes further analysis of this problem difficult. If tectonism or differential compaction is the reason for the observed relationship then run-up of the low-density turbidites that characterize Unit 1 would have acted to exaggerate the intra-formational onlap that was caused by tilting, and the underlying principles of this study are maintained. Unit 1 would therefore be analogous to the ponded aprons identified in intra-slope basins of the Gulf of Mexico, while Unit 2 would similar to a perched apron (Prather et al. 2017).

Turbidity current run-up and onlap geometry

Sediment gravity flows are able to flow significant distances up topography (e.g. Muck and Underwood, 1990; Lamb et al. 2008; Dorrell et al. 2018). The distance a turbidity current runs up topography is termed the run-up height (H) and, in its simplest form (following Straub et al. 2008) can be represented by:

$$(1)\ H = h + \frac{\rho_c U^2}{(\rho_c - \rho_a) 2g}$$

Where h = flow thickness, U = flow velocity, ρ_c = bulk density of the flow (composed of quartz at 2650 kg m^{-3}), ρ_a = density of the ambient water (seawater at 1020 kg m^{-3}), g = gravity (9.81 m s^{-1}). In order to

assign a single flow concentration value there is an assumption that there is no density stratification within the flow. A 30 m deep channel-form at Chambre du Roi (Sinclair, 2000) has been used as the basis for estimating minimum flow height. This is slightly arbitrary but serves the purpose of this 'thought experiment'. In order to correct for channel-related superelevation this flow height has been multiplied by 1.3 (see Mohrig & Buttles, 2007), giving a *h* value of 39 m. This height represents the minimum height of the flow at the lobe apex, disregards compaction, and is assumed constant. It should be noted that due to a lack of flow height proxies preserved at outcrop this value is used purely to demonstrate the underlying principles of the model, i.e. the model does not attempt to fully reconstruct the turbidity currents entering the Annot Basin. The depth-averaged flow velocities used range from 5 m s^{-1} to 0.5 m s^{-1}. The upper limit of 5 m s^{-1} is derived from the maximum flow velocities (4-6 m s^{-1}) reached by sand-rich flows in the Monterey Canyon (Symons et al. 2017), while the lower limit of 0.5 m s^{-1} is derived from average measurements of finer-grained flows in the Congo Canyon (Azpiroz-Zabala et al. 2017). The Annot system is sand-rich, therefore the faster Monterey flows are likely the most analogous, at least close to the input. Flow velocity will decrease with decreasing concentration, making the use of a constant velocity problematic. This is suggested to be less important for small and confined basins, such as the Annot Basin, where flows may be prevented from significant velocity decay between the axis and pinch-out. If velocities do decay significantly then plotting single velocity values through the height of an individual flow will be required, for example, the 5 ms^{-1} and 10% concentration basal part of a hypothetical flow will run-up 9.2 m above the flow height, while its 1 ms^{-1} and 0.1% concentration tail will run 32 m above the flow height. This decametre scale difference may explain the ~15 m of slope drape at Col du Fa (Fig. 6; 8). This parameter is further complicated by the possible presence of low-velocity dense basal layers within highly- concentrated stratified flows (e.g. Stevenson et al. 2018). Turbulence is suppressed in these basal layers, which reduces velocity and run-up heights, resulting in the increased likelihood of an abrupt pinch-out of the sand-rich basal layer and bypass of the upper and low-concentration parts of the flow. The 'wedged' high-density turbidites identified at onlap by this study (Fig. 11B) may be the depositional products of such basal layers.

By varying flow concentration in this equation, a clear trend is developed, with lower sediment concentrations resulting in greater run-up heights (Fig. 18A). In prograding lobe systems turbidity currents with lower sediment concentrations (well below 10%), forming low- or medium-density turbidites, are typically found in the distal or basal stratigraphy and flows with higher sediment concentrations (>10%), forming high-density turbidites, are typically found in the proximal or upper stratigraphy (e.g., Hodgson et al. 2006; 2009; this study). This therefore suggests that earliest turbulent flows into a receiving basin should have the greatest run-up heights, assuming all of these flows are of similar thickness, with run-up heights decreasing through time as flows become more concentrated (Fig. 18A). It should be noted that the effect of increasing concentration through time will be counter-acted by increasing velocities, as discussed previously. Suspended sediment concentrations of >~8% have been shown to suppress the generation of current ripples and cause transformation from turbulent to

transitional flow, where flows decelerate sufficiently, forming transitional or hybrid flow deposits (Baas et al. 2011). This concentration has therefore informed the placement of hybrid beds along the run-up height trend (Fig. 18A). It should be noted that Baas et al. (2011) emphasise that this value is dependent on flow velocity, grain size and sediment composition, and that the dimensionless Reynolds number is a much better predictor of flow phase. The results of this analysis fit with facies-dependant thinning rates compiled from 18 outcrop studies by Tőkés and Patacci (2018), with hybrid-beds having 1.3 to 2.8 times higher thinning rates than turbidites. Data collected in this study also support the compiled data of Tőkés and Patacci (2018), with thinner-bedded turbidites having lower thinning rates than thicker-bedded turbidites (Fig. 13). Similar trends have been reported from levee sandstones (DeVries and Lindholm. 1994).

Lateral vs Frontal Onlap

To assess the run-up variation between frontal and lateral onlap the velocity of the modeled flow was varied according to the incidence angle of the flow with the slope. It is assumed that the flow velocity will be at its maximum (5 m s^{-1} in this case) in the principal direction of travel, or an angle of incidence of 0°, and that the flow velocity will fall to 0 ms^{-1} perpendicular to its axis at an angle of incidence of 90° , i.e., when the flow is running perpendicular to the topography. In reality there will still be some lateral velocity, however for the purposes of this simple analysis it is assumed that this is negligible. The fastest flows occur at an angle of incidence of 0° or perpendicular to the slope (Fig. 18B). These flows therefore run further up the counter slope. Deposits of these flows would pinch-out higher up the frontal slope than the lateral slope (Fig. 18B; C). In the 5 ms^{-1} case the difference in run-up height between the frontal and lateral part of the flow is around 80 m. The difference is reduced within slower flows, such as those in finer-grained systems (Azpiroz-Zabala et al. 2017).

DISCUSSION

Stratigraphic evolution of onlap

Based on the similarity between facies transitions and associations seen within this confined basin and those within unconfined or weakly confined submarine lobes (Fig. 8; 10; 18) (e.g., Hodgson, 2009; Spychala et al., 2016; 2017), and the onlap termination styles shown by this study to be produced by the parent flows of these facies (Fig. 16; 18), a predictable stratigraphic evolution of flow termination styles at confined basin margins is proposed (Fig. 19).

Distal fringe.---Initially, onlap terminations will be characterized by draping of the slope as low-density turbidites of the lobe fringe are deposited (Fig. 17; 20; 21). This low-density turbidite drape is likely to be composed of fine-grained sand, silt, or mud, as fine-grained flows are much more capable of flow inflation and deposition high on the slope (Dorrell et al. 2018). Lobe fringe deposition will heal substantial amounts of basinal topography and form a dominantly aggradational sequence of thin-beds on the basin margin (Fig. 11A; 18; 20).

Proximal fringe.---Hybrid-beds and low-density turbidites of the proximal lobe fringe are then deposited into the basin as the system progrades (Fig. 19). These hybrid flows are more concentrated and will therefore have lower flow efficiencies when they encounter the slope, so will be unable to deposit as far up the slope as the underlying low-density turbidites of the distal lobe fringe (Fig. 17; 20). This will cause abrupt intra-formational onlap of these higher-concentration flows against the underlying lobe fringe deposits (Fig. 19). In the Annot Basin this is represented by proximal fringe deposits wedging out against the underlying distal fringe deposits (Fig. 11A; Fig. 15). The abruptness and complex 3D geometry of these terminations is enhanced by the combined potential for hybrid-bed development through long run-out cohesive flow transformation (e.g. Haughton et al. 2009), slope-induced flow transformation (e.g. Barker et al. 2008; Patacci et al. 2014; Bell et al. 2018) and flow-induced slope failures (e.g. McCaffrey and Kneller, 2001) (Fig. 16). This depositional pattern will be seen in cross-sections as a progressive migration of termination points towards the basin center (offlap) (Fig. 19) or a reduction in distance between successive onlapping termination points towards the basin margin. Sylvester et al. (2015) generated similar onlap trends using a geometric approach with subsidence and sediment supply as the variables.

Off-axis.---As progradation continues these hybrid-bed-prone proximal fringe deposits will be overlain by deposits of more proximal flows which have not decelerated to the same degree and hence are more turbulent and lower concentration, but sand-rich (Fig. 17; 20). The off-axis deposits will be able to drape the slope more effectively than the underlying hybrid-beds owing to their lower sediment concentrations (Fig. 19). This will result in progressive termination of their deposits higher up on the slope and either intra-formational onlap against the now thinner veneer of the low-density fringe, or onlap directly against the hemipelagic basin margin (Fig. 17; 22).

Axis.---As higher-concentration flows begin to dominate, intra-formational onlap may occur against the underlying fringe or off-axis deposits that were able to run-up the hemipelagic slope (Fig. 19). The highly concentrated basal layers of these flows will be preserved as abruptly onlapping high-density turbidites, with the low-density tail of the flow bypassed down-dip. These axial flows will also be more erosive and able to incorporate mud-rich substrate, resulting in an increasing likelihood of intra-formational onlap through short length-scale rheological flow transformation and consequent higher thinning rates adjacent to the basin margin (Fig. 15). The scours formed these erosive events close to onlap will promote further autocyclic modulation of stacking patterns adjacent to the basin margin (e.g. Eggenhuisen et al. 2011). This relationship will also be exaggerated in coarser-grained systems as higher concentration flows will be less able to deposit further up the slope, particularly at lateral margins if these high-concentration flows are narrower (Al-Jaidi et al. 2004).

A critical point in the basin fill will then be reached when these deposits sufficiently heal the confining topography to allow bypass of the coarser components of flows over the confining slope, forming a stepped, instead of ponded, basin (Prather et al. 2017). Until this level is reached the finer-grained parts of the flows were stripped, thus increasing the sand proportion in the up-dip basin (Prather

et al. 2017). This transition is represented toward the sill of the Annot Basin where proximal lobe axis deposits bypass down-dip to the Grand Coyer minibasin (Fig. 2; 3), where this stratigraphic evolution repeats within the next confined depocenter.

In the case that the topography is sufficient so as not to be healed by the underlying deposits, the lobe axis deposits will continue to onlap against the underlying deposits until the accommodation is sufficiently healed to allow the axial deposits to onlap against the hemipelagic basin margin or completely fill the basinal relief and behave as essentially unconfined deposits, resulting in down-lapping terminations (Fig. 19; 21). Apparent unconfinement in a vertical section may also occur if allogenic progradation (e.g. increasing sediment flux) does not keep pace with topographic healing. This will result in the axial sandstones rarely onlapping directly against the constantly retreating basin margin and instead depositing away from the slope and on the basin floor (e.g. Kneller and McCaffrey, 1999).

Applicability

Syn-depositionally deforming basins.---This general stratigraphic evolution applies most readily to static basins with little syn-depositional deformation, where onlap trends are not modified by changes in subsidence or depocentre migration (Fig. 21). The Annot Basin was subject to syn-depositional movement of the depocenter (e.g., Salles et al., 2014), however stratigraphic units of the basin fill show the same conceptual evolution as hypothesized for a static basin (Fig. 6), with the only difference being that the onlap is exaggerated on the tilted eastern exposures because of the increasing slope angle during deposition (Fig. 11A) (Salles et al. 2014). In salt-basins, where syn-depositional subsidence can be rapid, this onlap evolution will be also be exaggerated. The general model for flow termination evolution (Fig. 19) may therefore broadly apply to actively deforming basins (Fig. 21). It may be difficult, however, to differentiate between allogenic onlap patterns caused by syn-depositional subsidence or sediment flux (e.g. Sylvester et al., 2015) and those caused by autogenic variations in flow properties (Fig. 21). Care therefore needs to be taken when reconstructing tectonic histories from onlap trends alone, especially in datasets without lithological control.

Onlap incidence angle---Frontal onlap allows for greater run-up than lateral onlap (Fig. 18B, C). This in turn makes the model presented here more applicable for dip sections against a confining slope. This is further reinforced by the Le Ray dip-oblique correlation (Fig. 6), which is interpreted to record the stratigraphic evolution of onlap described. The lack of a significant thin-bedded slope drape at the lateral onlap of Grès d'Annot at Chalufy (e.g. Puigdefabregas et al. 2004; Smith and Joseph, 2004) may be an example of the importance of incidence angle, with run-up decreased against the lateral slope (Fig. 18B; C). A minor thin-bedded slope drape does exist at Chalufy, however, and intra-formational onlap does occur against these thin-beds (e.g. Bakke et al. 2013). This relationship may occur against lateral margins because flows become increasingly elongate with increasing sediment concentrations (Al-Jaidi et al. 2004). In strike-sections this will result in a similar onlap termination pattern, with thicker and

lower concentration flows of the lobe fringe depositing higher on the lateral slope than higher concentration flows of the lobe axis, which are elongated in the dip-direction and more prone to bypass down-dip. This relationship may therefore apply to both strike and dip exposures, however greater understanding of frontal vs lateral onlap in exposed or subsurface deep-water systems is required for further analysis.

Hierarchical scale.--- The onlap termination patterns observed in this study are mainly seen on the scale of 10s of metres, similar to typical lobe or possibly lobe complex dimensions (Prélat et al. 2009). Above the spatio-temporal scale of lobe complexes the morphology of the depositional element is less likely to be the result of autogenic processes acting on individual events and more likely to be controlled by allogenic factors, such as the interplay of basin subsidence and sediment supply (see 'stratigraphic interval scale' of Sheets et al. 2002; Jobe et al. 2018) (Fig. 21). It should be noted that in confined basins established morphometric ranges for unconfined depositional element thicknesses breakdown due to variable degrees of confinement across systems (Prélat et al. 2010). The lobe-scale applicability of the model is therefore purely a hierarchical observation as lobe thicknesses will vary across systems.

Stratigraphic position.--- Lobe progradation is unlikely to be constant and will show small-scale backstepping (Fig. 17), interpreted to be due to high-frequency sea level fluctuations or periods of starved sediment delivery. This backstepping creates discrete boundaries between successive members in the Annot Basin (Callec et al. 2004) (Fig. 5). These fluctuations will result in a non-uniform flow concentration evolution during progradation, however on the basin-scale the overall trend of increasing flow concentration and subsequent onlap termination style will be maintained, with higher-density flows becoming more prevalent in the basin through progradation. These observations make the model most applicable to the early fill of confined deep-water systems, where confinement is greatest and distal thin-bedded turbidites will be most prevalent.

Low-density and thin-bedded turbidites also tend to form thinner successions than high-density and thick-bedded turbidites. This is because sediment volume and sedimentation rates are greater in higher-density flows and because differential compaction more heavily affects finer-grained successions. This has implications for the evolution of onlap because the distal lobe fringe will be thinner than the lobe axis. As a result, the intra-formational onlap against the underlying fringe will be much more difficult to detect through time as the draping low-density turbidites gradually become thinner as the basin fills, eventually resulting in the higher-density flows onlapping directly against the hemipelagic basin margin (Fig. 17; 20; 22). This relationship is seen within Le Ray (Fig. 6), where the thin-bedded fringe is gradually surmounted by later flows.

CONCLUSION

Understanding flow interaction with, and bed termination against, confining topography is critical for reconstructing the structural and sedimentological evolution of deep-water basins. This study

presents a review of onlap termination styles in deep-water settings based on detailed field investigations (Fig. 14) and compares these results against those from a simple numerical model (Fig. 16). Onlap terminations are shown to evolve in a predictable way through the progradation of a submarine lobe succession (Fig. 14; 16; 18; 19), with different lobe sub-environments (Table 1) identified at the basin margin through the migration of successive termination points and facies trends (Fig. 16; 18).

Initially termination points migrate towards the basin margins as low-density turbidites significantly drape the inherited basinal topography. Progressively higher magnitude flows with greater sediment concentrations of the hybrid bed-rich proximal fan fringe onlap these underlying deposits causing the development of an intra-formational onlap surface that is characterized by either a basinward shift in termination points or a reduced distance between successive termination points towards the basin margin. Hybrid-beds are also shown to constitute significant thicknesses of the proximal fringe in confined systems through long run-out transformation, slope-induced transformation, and intra-basinal slope instability. Progradation of the lobe off-axis over the proximal fringe will cause further intra-formational onlap as the lower-concentration off-axis deposits drape the slope. Onlap against the fringe drape will continue until it is surmounted and onlap occurs directly against the hemipelagic basin margin. Intra-formational onlap may also occur in the lobe axis through abrupt onlap of these high-concentration deposits against the underlying lower-concentration fringe or off-axis deposits. These autogenic processes act to modulate the allogenic signature of progradation in the Annot Basin, with apparent back-stepping of the sand-rich component of the system not necessarily representing allogenic retrogradation. This apparent back-stepping may instead be caused by the interaction between longitudinal flow evolution and confining basin margins. Depositional hierarchy is also shown to be important when interpreting onlap patterns, with autogenic processes more important at the lobe-scale and allogenic processes more important at the lobe-complex scale.

REFERENCES

AL JA'AIDI, O.S., MCCAFFREY, W.D. AND KNELLER, B.C, 2004, Factors influencing the deposit geometry of experimental turbidity currents: implications for sand-body architecture in confined basins. Geological Society, London, Special Publications, v. 222, p. 45–58.

AMY, L.A., MCCAFFREY, W.D. AND KNELLER, B.C., 2004, The influence of a lateral basin-slope on the depositional patterns of natural and experimental turbidity currents. Geological Society, London, Special Publications: v. 221, p. 311-330.

AMY, L.A., TALLING, P.J., PEAKALL, J., WYNN, R.B. AND THYNNE, R.A., 2005, Bed geometry used to test recognition criteria of turbidites and (sandy) debrites: Sedimentary Geology, v. 179, p. 163-174.

APPS, G, 1987, Evolution of the Grès d'Annot Basin, SW Alps: Ph.D. thesis, University of Liverpool.

APPS, G., PEEL, F. AND ELLIOTT, T., 2004, The structural setting and palaeogeographical evolution of the Grès d'Annot basin. Geological Society, London, Special Publications: v. 221, p. 65-96.

AZPIROZ-ZABALA, M., CARTIGNY, M.J., TALLING, P.J., PARSONS, D.R., SUMNER, E.J., CLARE, M.A., SIMMONS, S.M., COOPER, C. AND POPE, E.L., 2017, Newly recognized turbidity current structure can explain prolonged flushing of submarine canyons: Science Advances, v. 3, p. e1700200.

BAAS, J.H., BEST, J.L. AND PEAKALL, J., 2011, Depositional processes, bedform development and hybrid bed formation in rapidly decelerated cohesive (mud–sand) sediment flows: Sedimentology, v. 58, p. 1953-1987.

BARKER, S.P., HAUGHTON, P.D.W., MCCAFFREY, W.D., ARCHER, S.G., AND HAKES, B, 2008, Development of rheological heterogeneity in clay-rich high-density turbidity currents: Aptian Britannia Sandstone Member, UK continental shelf: Journal of Sedimentary Research, v. 78, p. 45–68.

BAKKE, K., KANE, I.A., MARTINSEN, O.J., PETERSEN, S.A., JOHANSEN, T.A., HUSTOFT, S., JACOBSEN F.H. AND GROTH, A., 2013, Seismic modeling in the analysis of deep-water sandstone termination styles: AAPG bulletin, v. 97, p. 1395-1419.

BEAUBOUEF, R.T. AND FRIEDMANN, S.J., 2000, December. High resolution seismic/sequence stratigraphic framework for the evolution of Pleistocene intra slope basins, western Gulf of Mexico: depositional models and reservoir analogs. In: Deep-water reservoirs of the world: Gulf Coast Section SEPM 20th Annual Research Conference, p. 40-60.

BRUNT, R.L., MCAFFREY, W.D. AND KNELLER, B.C., 2004, Experimental modeling of the spatial distribution of grain size developed in a fill-and-spill mini-basin setting. Journal of Sedimentary Research: v. 74, p. 438-446.

BOULESTEIX, K., POYATOS-MORE, M., FLINT, S.S., TAYLOR, K., HODGSON, D.M., AND HASIOTIS, T. M., 2019, Transport and deposition of mud in deep-water environments: processes and stratigraphic implications: Sedimentology, in press.

BOUMA, A. H., 1962, Sedimentology of Some Flysch Deposits: A Graphic Approach to Facies Interpretation: New York: Elsevier. 168 p.

CALLEC, Y., 2004, The turbidite fill of the Annot sub-basin (SE France): a sequence-stratigraphy approach: Geological Society, London, Special Publications, v. 221, p. 111-135.

CLARK, J.D. AND STANBROOK, A., 2001, Formation of large-scale shear structures during deposition from high-density turbidity currents, Grès d'Annot Formation, south-east France: Particulate Gravity Currents, v. 31, p. 219-232.

COVAULT, J.A. AND ROMANS, B.W., 2009, Growth patterns of deep-sea fans revisited: Turbidite-system morphology in confined basins, examples from the California Borderland: Marine Geology, v. 265, p. 51-66.

CUNHA, R.S., TINTERRI, R. AND MAGALHAES, P.M., 2017, Annot Sandstone in the Peïra Cava basin: An example of an asymmetric facies distribution in a confined turbidite system (SE France). Marine and Petroleum Geology, v. 87, p. 60-79.

DEPTUCK, M.E., PIPER, D.J., SAVOYE, B. AND GERVAIS, A., 2008, Dimensions and architecture of late Pleistocene submarine lobes off the northern margin of East Corsica: Sedimentology, v. 55(4), p. 869-898.

DEVRIES, M. AND LINDHOLM, R.M., 1994, Internal architecture of a channel– levee complex, Cerro Toro Formation, Southern Chile. *in* Weimer, P., Bouma, A.H., Perkins, B.F., eds., Submarine Fans and Turbidite Systems GCSSEPM Foundation, Houston, p. 105–114.

DORRELL, R.M., PATACCI, M., MCCAFFREY, W. D., Inflation of Ponded, Particulate Laden Density Currents: Journal of Sedimentary Research, v. 88(11), p. 1276–1282.

DOUGHTY-JONES, G., MAYALL, M. AND LONERGAN, L., 2017, Stratigraphy, facies, and evolution of deep-water lobe complexes within a salt-controlled intraslope minibasin: AAPG Bulletin, v. 101, p. 1879-1904.

DU FORNEL, E., JOSEPH, P., DESAUBLIAUX, G., ESCHARD, R., GUILLOCHEAU, F., LERAT, O., MULLER, C., RAVENNE, C. AND SZTRAKOS, K., 2004, The southern Grès d'Annot outcrops (French Alps): an attempt at regional correlation: Geological Society, London, Special Publications, v. 221, p. 137-160.

EGGENHUISEN, J.T., MCCAFFREY, W.D., HAUGHTON, P.D. AND BUTLER, R.W., 2011, Shallow erosion beneath turbidity currents and its impact on the architectural development of turbidite sheet systems: Sedimentology, v. *58*(4), p. 936-959.

ETUORI, T., APPS, G., DAVIES, H., EVANS, M., GHIBAUDO, G., AND GRAHAM, R.H., 1985, A structural and sedimentological traverse through the Tertiary foreland basin of the external Alps of south-east France, in Allen, P.A., and Homewood, P. (eds.): Field Excursion Guidebook for the International Association of Sedimentologists Meeting on Foreland Basins in Fribourg, p. 39-73.

GARDINER, A.R., 2006, The variability of turbidite sandbody pinchout and its impact on hydrocarbon recovery in stratigraphically trapped fields: Geological Society, London, Special Publications, v. 254, p. 267-287.

GERVAIS, A., SAVOYE, B., PIPER, D.J., MULDER, T., CREMER, M. AND PICHEVIN, L., 2004, Present morphology and depositional architecture of a sandy confined submarine system: the Golo turbidite system (eastern margin of Corsica): Geological Society, London, Special Publications, v. 222(1), p. 59-89.

GRUNDVÅG, S.A., JOHANNESSEN, E.P., HELLAND-HANSEN, W. AND PLINK-BJÖRKLUND, P., 2014, Depositional architecture and evolution of progradationally stacked lobe complexes in the Eocene Central Basin of Spitsbergen: Sedimentology, v. 61(2), p. 535-569.

HAUGHTON, P. D. W., 1994, Deposits of deflected and ponded turbidity currents, Sorbas basin, Southeast Spain: Journal of Sedimentary Research, v. 64, p. 233–246.

HAUGHTON, P.D., 2000, Evolving turbidite systems on a deforming basin floor, Tabernas, SE Spain: Sedimentology, v. 47, p. 497-518.

HAUGHTON, P.D., BARKER, S.P. AND MCCAFFREY, W.D., 2003, 'Linked'debrites in sand-rich turbidite systems–origin and significance: Sedimentology, v. 50, p. 459-482.

HAUGHTON, P., DAVIS, C., MCCAFFREY, W. AND BARKER, S., 2009, Hybrid sediment gravity flow deposits–classification, origin and significance: Marine and Petroleum Geology, v. 26. P. 1900-1918.

HISCOTT, R.N., 1994, Loss of capacity, not competence, as the fundamental process governing deposition from turbidity currents: Journal of Sedimentary Research, v. 64, p. 209–214.

HODGSON, D.M. AND HAUGHTON, P.D., 2004, Impact of syndepositional faulting on gravity current behaviour and deep-water stratigraphy: Tabernas-Sorbas Basin, SE Spain: Geological Society, London, Special Publications, v. 222, p. 135-158.

HODGSON, D.M., 2009, Distribution and origin of hybrid beds in sand-rich submarine fans of the Tanqua depocenter, Karoo Basin, South Africa: Marine and Petroleum Geology, v. 26, p. 1940-1956.

HODGSON, N.A., FARNSWORTH, J. AND FRASER, A.J., 1992, Salt-related tectonics, sedimentation and hydrocarbon plays in the Central Graben, North Sea, UKCS: Geological Society, London, Special Publications, v. 67, p. 31-63.

FONNESU, M., HAUGHTON, P., FELLETTI, F. AND MCCAFFREY, W., 2015, Short length-scale variability of hybrid event beds and its applied significance: Marine and Petroleum Geology, v. 67, p. 583-603.

FONNESU, M., FELLETTI, F., HAUGHTON, P.D., PATACCI, M. AND MCCAFFREY, W.D., 2018, Hybrid event bed character and distribution linked to turbidite system sub-environments: The North Apennine Gottero Sandstone (north-west Italy): Sedimentology, v. 65(1), p. 151-190.

FORD, M., LICKORISH, W. AND KUSNIR, N., 1999, Tertiary foreland sedimentation in the southern subalpine chains, SE France: a geodynamic appraisal: Basin Research, v. 11, p. 315-336.

KANE, I.A., KNELLER, B.C., DYKSTRA, M., KASSEM, A. AND MCCAFFREY, W.D., 2007, Anatomy of a submarine channel–levee: an example from Upper Cretaceous slope sediments, Rosario Formation, Baja California, Mexico: Marine and Petroleum Geology, v. 24, p. 540-563.

KANE, I.A., CATTERALL, V., MCCAFFREY, W.D. AND MARTINSEN, O.J., 2010, Submarine channel response to intrabasinal tectonics: The influence of lateral tilt: AAPG bulletin, v. 94, p. 189-219.

KANE, I.A AND PONTÉN, A.S., 2012, Submarine transitional flow deposits in the Paleogene Gulf of Mexico: Geology, v. 40, p. 1119-1122.

KANE, I.A., PONTÉN, A.S., VANGDAL, B., EGGENHUISEN, J.T., HODGSON, D.M. AND SPYCHALA, Y.T., 2017, The stratigraphic record and processes of turbidity current transformation across deep-marine lobes: Sedimentology, v. 64, p. 1236-1273.

KILHAMS, B., HARTLEY, A., HUUSE, M. AND DAVIS, C., 2012, Characterizing the Paleocene turbidites of the North Sea: the Mey Sandstone Member, Lista Formation, UK Central Graben. Petroleum Geoscience, v. 18(3), p. 337-354.

KNELLER, B. C., EDWARDS, D., MCCAFFREY, W. D. AND MOORE, R., 1991, Oblique reflection of turbidity currents: Geology, v. 19, p. 250 252.

KNELLER, B. C., 1995, Beyond the turbidite paradigm: physical models for deposition of turbidites and their implications for reservoir prediction. *in* Hartley, A. and Prosser, D. J., eds., Characterisation of Deep Marine Clastic Systems, Geological Society, London, Special Publications, v. 94, p. 29-46.

KNELLER, B.C. AND MCCAFFREY, W.D., 1995, Modelling the effects of salt-induced topography on deposition from turbidity currents: Society of Economic Palaeontologists and Mineralogists, Gulf Coast Section, p. 137-145.

KNELLER, B. C. AND MCCAFFREY, W. D., 1999, Depositional effects of flow non-uniformity and stratification within turbidity currents approaching a bounding slope: deflection, reflection and facies variation: Journal of Sedimentary Research, v. 69, p. 980-991.

KNELLER, B., 2003, The influence of flow parameters on turbidite slope channel architecture. Marine and Petroleum Geology, v. 20, p. 901-910.

KNELLER, B., DYKSTRA, M., FAIRWEATHER, L. AND MILANA, J.P., 2016, Mass-transport and slope accommodation: Implications for turbidite sandstone reservoirs: AAPG Bulletin, v. 100, p. 213-235.

KUBO, Y.S., 2004, Experimental and numerical study of topographic effects on deposition from two-dimensional, particle-driven density currents: Sedimentary Geology, v. 164, p. 311-326.

JACKSON, C.A.L., BARBER, G.P. AND MARTINSEN, O.J., 2008, Submarine slope morphology as a control on the development of sand-rich turbidite depositional systems: 3D seismic analysis of the Kyrre Fm (Upper Cretaceous), Måløy Slope, offshore Norway: Marine and Petroleum Geology, v. 25(8), p. 663-680.

JACKSON, C.A.L., ZAKARIA, A.A., JOHNSON, H.D., TONGKUL, F. AND CREVELLO, P.D., 2009, Sedimentology, stratigraphic occurrence and origin of linked debrites in the West Crocker Formation (Oligo-Miocene), Sabah, NW Borneo: Marine and Petroleum Geology, v. 26, p. 1957-1973.

JOBE, Z.R., SYLVESTER, Z., HOWES, N., PIRMEZ, C., PARKER, A., CANTELLI, A., SMITH, R., WOLINSKY, M.A., O'BYRNE, C., SLOWEY, N. AND PRATHER, B., 2017, High-resolution, millennial-scale patterns of bed compensation on a sand-rich intraslope submarine fan, western Niger Delta slope: GSA Bulletin, v. 129, p. 23-37.

JOSEPH, P. AND LOMAS, S.A., 2004, Deep-water sedimentation in the Alpine Foreland Basin of SE France: New perspectives on the Grès d'Annot and related systems—an introduction: Geological Society, London, Special Publications, v. 221, p. 1-16.

LAMB, M.P., PARSONS, J.D., MULLENBACH, B.L., FINLAYSON, D.P., ORANGE, D.L. AND NITTROUER, C.A., 2008, Evidence for superelevation, channel incision, and formation of cyclic steps by turbidity currents in Eel Canyon, California: Geological Society of America Bulletin, v. 120, p. 463-475.

LEE, S.E., AMY, L.A. AND TALLING, P.J., 2004, The character and origin of thick base-of-slope sandstone units of the Peïra Cava outlier, SE France: Geological Society, London, Special Publications, v. 221, p. 331-347.

LIU, Q., KNELLER, B., FALLGATTER, C., VALDEZ BUSO, V. AND MILANA, J.P., 2018. Tabularity of individual turbidite beds controlled by flow efficiency and degree of confinement: Sedimentology, Available online.

LOMAS, S.A. AND JOSEPH, P., 2004, Confined turbidite systems: Geological Society, London, Special Publications, v. 222, p. 1-7.

LOWE, D.R., 1982, Sediment gravity flows: II Depositional models with special reference to the deposits of high-density turbidity currents: Journal of Sedimentary Research, v. 52. p. 279-297.

LOWE, D.R. AND GUY, M., 2000, Slurry-flow deposits in the Britannia Formation (Lower Cretaceous), North Sea: a new perspective on the turbidity current and debris flow problem: Sedimentology, v. 47, p. 31-70.

MARINI, M., PATACCI, M., FELLETTI, F. AND MCCAFFREY, W.D., 2016, Fill to spill stratigraphic evolution of a confined turbidite mini-basin succession, and its likely well bore expression: The Castagnola Fm, NW Italy: Marine and Petroleum Geology, v. 69, p. 94-111.

MAYALL, M., LONERGAN, L., BOWMAN, A., JAMES, S., MILLS, K., PRIMMER, T., POPE, D., ROGERS, L. AND SKEENE, R., 2010, The response of turbidite slope channels to growth-induced seabed topography: AAPG Bulletin, v. 94(7), p. 1011-1030.

MCCAFFREY, W. D AND KNELLER, B. C., 2001, Process controls on the development of stratigraphic trap potential on the margins of confined turbidite systems and aids to reservoir evaluation: AAPG Bulletin, v. 85, p. 971-988.

MIDDLETON, G.V. AND HAMPTON, M.A., 1973, Sediment gravity flows: Mechanics of flow and deposition. *in* Middleton, G.V., Bouma, A.H., eds., Turbidites and deep water sedimentation: Pacific Section. Society of Economic Paleontologists and Mineralogists Book 2, Short Course Notes, 1–38.

MOUGIN, F., 1978, Contribution h l'Etude des Sediments Tertiaires de la Partie Orientale du Synclinal d'Annot (Alpes de Haute Provence). Stratigraphie, Grochimie, Micropaldontologie: Unpublished Ph.D. Thesis, Universiti Scientifique et Medicale de Grenoble, Grenoble.

MUTTI, E., BERNOULLI, D., LUCCHI, F.R. AND TINTERRI, R., 2009. Turbidites and turbidity currents from Alpine 'flysch'to the exploration of continental margins: Sedimentology, v. 56(1), p. 267-318.

MUCK, M.T. AND UNDERWOOD, M.B., 1990, Upslope flow of turbidity currents: A comparison among field observations, theory, and laboratory models: Geology, v. 18, p. 54-57

MULDER, T. AND ALEXANDER, J., 2001, The physical character of subaqueous sedimentary density flows and their deposits: Sedimentology, v. 48, p. 269-299.

OLUBOYO, A.P., GAWTHORPE, R.L., BAKKE, K. AND HADLER-JACOBSEN, F., 2014. Salt tectonic controls on deep-water turbidite depositional systems: Miocene, southwestern Lower Congo Basin, offshore Angola: Basin Research, v. 26, p. 597-620.

ORTIZ-KARPF, A., HODGSON, D.M. AND MCCAFFREY, W.D., 2015, The role of mass-transport complexes in controlling channel avulsion and the subsequent sediment dispersal patterns on an active margin: the Magdalena Fan, offshore Colombia: Marine and Petroleum Geology, v. 64, p. 58-75.

ORTIZ-KARPF, A., HODGSON, D.M., JACKSON, C.A.L. AND MCCAFFREY, W.D., 2016, Mass-Transport Complexes as Markers of Deep-Water Fold-and-Thrust Belt Evolution: Insights from the Southern Magdalena Fan, Offshore Colombia: Basin Research, v. 30, p. 65-88.

PATACCI, M., HAUGHTON, P.D. AND MCCAFFREY, W.D., 2014, Rheological complexity in sediment gravity flows forced to decelerate against a confining slope, Braux, SE France. Journal of Sedimentary Research, v. 84, p. 270-277.

PICKERING, K.T. AND HISCOTT, R.N., 1985, Contained (reflected) turbidity currents from the Middle Ordovician Cloridorme Formation, Quebec, Canada: an alternative to the antidune hypothesis: Sedimentology, v. 32, p. 373-394.

PINTER, P.R., BUTLER, R.W., HARTLEY, A.J., MANISCALCO, R., BALDASSINI, N. AND DI STEFANO, A., 2017, Tracking sand-fairways through a deformed turbidite system: the Numidian (Miocene) of Central Sicily, Italy: Basin Research, v. 30, p. 480-501.

PRATHER, B. E., BOOTH, J. R., STEFFENS, G. S. & CRAIG, P. A., 1998, Classification, lithologic calibration, and stratigraphic succession of seismic facies of intraslope basins, deep-water Gulf of Mexico:. AAPG Bulletin, v. 82, p. 701-728.

PRATHER, B.E., PIRMEZ, C., WINKER, C.D., 2012, Stratigraphy of linked intraslope basins: Brazos-Trinity system western Gulf of Mexico. Application of the principles of seismic geomorphology to continental-slope and base-of-slope systems: Case studies from seafloor and near-seafloor analogues: SEPM, Special Publication, v. 99, p. 83-109.

PRATHER, B.E., O'BYRNE, C., PIRMEZ, C. AND SYLVESTER, Z., 2017. Sediment partitioning, continental slopes and base-of-slope systems: Basin Research, v. 29(3), p. 394-416.PRÉLAT, A., HODGSON, D.M. AND FLINT, S.S., 2009, Evolution, architecture and hierarchy of distributary deep-water deposits: a high-resolution outcrop investigation from the Permian Karoo Basin, South Africa: Sedimentology, v. 56, p. 2132-2154.

PRÉLAT, A., COVAULT, J.A., HODGSON, D.M., FILDANI, A. AND FLINT, S.S., 2010, Intrinsic controls on the range of volumes, morphologies, and dimensions of submarine lobes: Sedimentary Geology, v. 232, p. 66-76.

PUIGDEFÀBREGAS, C., GJELBERG, J.M. AND VAKSDAL, M., 2004, The Grès d'Annot in the Annot syncline: outer basin-margin onlap and associated soft-sediment deformation: Geological Society, London, Special Publications, v. 221, p. 367-388.

RAVENNE, C., RICHE, P., TREMOLIERES, P. AND VIALLY, R., 1987, Sédimentation et tectonique dans le bassin marin Eocène supérieur-Oligocène des Alpes du Sud: Revue de l'Institut Français du Pétrole, v. 42(5), p. 529-553.

SALLES, L., FORD, M., JOSEPH, P., DE VESLUD, C.L.C. AND LE SOLLEUZ, A., 2011, Migration of a synclinal depocenter from turbidite growth strata: the Annot syncline, SE France: Bulletin de la Société Géologique de France, v. 182, p. 199-220.

SALLES, L., FORD, M. AND JOSEPH, P., 2014, Characteristics of axially-sourced turbidite sedimentation on an active wedge-top basin (Annot Sandstone, SE France): Marine and Petroleum Geology, v. 56, p. 305-323.SINCLAIR , H. D., 1994, The influence of lateral basin slopes on turbidite sedimentation in the Annot Sandstones of SE France: Journal of Sedimentary Research, v. 64, p. 42-54.

SHEETS, B.A., HICKSON, T.A. AND PAOLA, C., 2002, Assembling the stratigraphic record: depositional patterns and time-scales in an experimental alluvial basin: Basin Research, v. 14(3), p. 287-301.

SINCLAIR, H.D., 1997, Tectonostratigraphic model for underfilled peripheral foreland basins: An Alpine perspective: Geological Society of America Bulletin, v. 109, p. 324-346

SINCLAIR, H.D., 2000, Delta-fed turbidites infilling topographically complex basins: a new depositional model for the Annot Sandstones, SE France: Journal of Sedimentary Research, v. 70, p. 504–519.

SINCLAIR, H.D. AND TOMASSO, M., 2002, Depositional evolution of confined turbidite basins: Journal of Sedimentary Research, p. 72, v. 451-456.

SOUTHERN, S.J., PATACCI, M., FELLETTI, F. AND MCCAFFREY, W.D., 2015, Influence of flow containment and substrate entrainment upon sandy hybrid event beds containing a co-genetic mud-clast-rich division: Sedimentary Geology, p. 321, v. 105-122.

SOUTTER, E.L., KANE, I.A. AND HUUSE, M., 2018, Giant submarine landslide triggered by Paleocene mantle plume activity in the North Atlantic: Geology, v. 46(6), p. 511-514.

STANBROOK, D.A. AND CLARK, J.D., 2004, The Marnes Brunes Inférieures in the Grand Coyer remnant: characteristics, structure and relationship to the Grès d'Annot: Geological Society, London, Special Publications, p. 221, v. 285-300.

STANLEY, D.J. AND MUTTI, E., 1968, Sedimentological evidence for an emerged land mass in the Ligurian sea during the Palaeogene: Nature, v. 218(5136), p.32.

STANLEY, D.J., 1980, The Saint-Antonin conglomerate in the Maritime Alps: a model for coarse sedimentation on a submarine slope: Smithsonian Contributions to the Marine Sciences, v. 5, p. 1–25.

SMITH, R.U., 2004, Silled sub-basins to connected tortuous corridors: sediment distribution systems on topographically complex sub-aqueous slopes: Geological Society, London, Special Publications, v. 222, p. 23-43.

SMITH, R., 2004. Turbidite systems influenced by structurally induced topography in the multi-sourced Welsh Basin: Geological Society, London, Special Publications, v. 222, p. 209-228.

SMITH, R. AND JOSEPH, P., 2004, Onlap stratal architectures in the Grès d'Annot: Geometric models and controlling factors: Geological Society, London, Special Publications, v. 221(1), p. 389-399

STRAUB, K.M., MOHRIG, D., MCELROY, B., BUTTLES, J. AND PIRMEZ, C., 2008, Interactions between turbidity currents and topography in aggrading sinuous submarine channels: A laboratory study: GSA Bulletin, v. 120, p. 368-385.

SPYCHALA, Y.T., HODGSON, D.M., FLINT, S.S. AND MOUNTNEY, N.P., 2015, Constraining the sedimentology and stratigraphy of submarine intraslope lobe deposits using exhumed examples from the Karoo Basin, South Africa: Sedimentary Geology, v. 322, p. 67-81.

SPYCHALA, Y.T., HODGSON, D.M., STEVENSON, C.J. AND FLINT, S.S., 2016, Aggradational lobe fringes: The influence of subtle intrabasinal seabed topography on sediment gravity flow processes and lobe stacking patterns. Sedimentology., v. 64, p. 582-608.

SPYCHALA, Y.T., HODGSON, D.M., PRÉLAT, A., KANE, I.A., FLINT, S.S. AND MOUNTNEY, N.P., 2017, Frontal and lateral submarine lobe fringes: comparing sedimentary facies, architecture and flow processes: Journal of Sedimentary Research, v. 87, p. 75-96.

STEVENSON, C.J., JACKSON, C.A.L., HODGSON, D.M., HUBBARD, S.M. AND EGGENHUISEN, J.T., 2015, Deep-water sediment bypass: Journal of Sedimentary Research, v. 85, p. 1058-1081.

STEVENSON, C.J., FELDENS, P., GEORGIOPOULOU, A., SCHÖNKE, M., KRASTEL, S., PIPER, D.J., LINDHORST, K. AND MOSHER, D., 2018, Reconstructing the sediment concentration of a giant submarine gravity flow: Nature communications, v. 9(1), p. 2616.

SYLVESTER, Z., CANTELLI, A. AND PIRMEZ, C., 2015, Stratigraphic evolution of intraslope minibasins: Insights from surface-based model: AAPG Bulletin, v. 99, p. 1099-1129.

SYMONS, W.O., SUMNER, E.J., PAULL, C.K., CARTIGNY, M.J., XU, J.P., MAIER, K.L., LORENSON, T.D. AND TALLING, P.J., 2017, A new model for turbidity current behavior based on integration of flow monitoring and precision coring in a submarine canyon: Geology, v. 45, p. 367-370.

TALLING, P.J., AMY, L.A. AND WYNN, R.B., 2007, New insight into the evolution of large-volume turbidity currents: comparison of turbidite shape and previous modelling results: Sedimentology, v. 54(4), p.737-769.

TINTERRI, R., MAGALHAES, P.M., TAGLIAFERRI, A. AND CUNHA, R.S., 2016, Convolute laminations and load structures in turbidites as indicators of flow reflections and decelerations against bounding slopes. Examples from the Marnoso-arenacea Formation (northern Italy) and Annot Sandstones (south eastern France): Sedimentary Geology, v. 344, p. 382-407.

TŐKÉS, L. AND PATACCI, M., 2018. Quantifying tabularity of turbidite beds and its relationship to the inferred degree of basin confinement: Marine and Petroleum Geology, in press.

TOMASSO, M AND SINCLAIR, H.D., 2004, Deep-water sedimentation on an evolving fault-block: the Braux and St Benoit outcrops of the Grès d'Annot: Geological Society, London, Special Publications, v. 221, p. 267-283.

WALTHER, J., 1894, Einleitung in die Geologie als historische Wissenschaft. In: Lithogenesis der Gegenwart. Jena: G. Fischer, v. 3, p. 535–1055.

WEIMER, P. AND LINK, M.H., 1991, Global petroleum occurrences in submarine fans and turbidite systems. *in* Seismic facies and sedimentary processes of submarine fans and turbidite systems, Springer, New York, NY, p. 9-67.

WYNN, R.B., MASSON, D.G., STOW, D.A. AND WEAVER, P.P., 2000, The Northwest African slope apron: a modern analogue for deep-water systems with complex seafloor topography: Marine and Petroleum Geology, v. 17(2), p. 253-265.

FIGURE CAPTIONS

Fig. 1: A) Examples of onlap termination styles (modified from Bakke et al. 2014; Patacci et al. 2014). **B)** Generalised relationship between flow concentration and onlap geometry (modified from Bakke et al. 2013). t = time.

Fig. 2: Location, geological setting and exposure of the Cenozoic foreland basin of the Western Alps. The Late Eocene paleogeography is overlain (modified from Joseph and Lomas, 2004 and Salles et al. 2014) and the shows the Annot Basin (red box) located within the clastic submarine fan prograding northwards. Red line indicates boundary between terrestrial and marine environments. RF; Rouaine Fault. Blue arrows indicate paleoflow and blue lines indicate schematic fluvial systems.

Fig. 3: Structure and geological map of the Annot Basin (modified from Puidgefabregas et al., 2004 and Salles et al. 2014). The various anticlines confine deposition across the Basin. The clastic sequence has been divided into members based on aerial and outcrop mapping (modified from Puigdefabregas et al.,

2004; Salles et al., 2014). An attempt has been to reconcile the member sub-divisions used by Puigdefabregas et al. (2004) and Salles et al. 2014). White boxes indicate logged localities. White line indicates correlated panel on Figure. 5.

Fig. 4: Dip (A) and strike (B) field sketches of the stratigraphy and structure of the Annot Basin. Logged localities are shown as red traverses on (A).

Fig. 5: Dip-oblique correlation panel along the eastern margin of the Annot Basin. No horizontal scale. Localities and panel orientation on Fig. 3. Members have been correlated based on published maps and lithological observations. Paleocurrent data is associated with one sedimentary log or series of logs from one locality. The vertical thickness represents the exposed stratigraphy along the correlated margin (see Fig. 3 for location) and does not represent the accommodation of the entire basin, which had a westerly-migrating depocentre. This migration is represented within the eastern exposures by decreasing member thicknesses through time. It should also be noted that the due to the oblique nature of the correlation the margin position is a representation of the relative confinement on a member-scale and does not indicate onlap angle.

Fig. 6: Correlation panel for the Le Ray member within the Annot Basin. Paleoflow is from the left to right (south to north).

Table 1: Key lithofacies, facies associations and onlap geometries seen within the Annot Basin.

Fig. 7: Correlation panel from the Col du Fa outcrop. The thinner-bedded low-density turbidites drape and heal the topography of the Marnes Bleues basin margin onlap surface, while the higher-density and thicker-bedded turbidites initially onlap against these distal deposits, forming an intra-formational onlap surface. Red lines on x-axis indicate exact log position.

Fig. 8: A) Nomenclature comparison between unconfined lobe sub-environments (Spychala et al. 2017) and **B)** confined lobe sub-environments. The only difference suggested is that hybrid-beds are more prevalent in lateral positions within confined systems due to rapid flow deceleration and transformation at basin margins. LDT = low-density turbidite; HEB = hybrid (event) bed; MDT = medium-density turbidite; HDT = high-density turbidite. Unconfined and confined lobe dimensions from Prelat et al. (2010) (rounded to nearest 10 km).

Fig. 9: Sedimentary logs with facies and paleogeographical interpretations. Each member contains elements of each lobe sub-environment, however there is an increasing prevalence of higher-density deposits upwards through stratigraphy. This pattern is interpreted as representing overall lobe progradation. Coloured bars next to logs represent facies on sub-environment key.

Fig. 10 A) MDT at Col du Fa. **B)** LDT onlapping a gravel lag deposit at Tête du Ruch (Lower). **C)** Organic material within debritic division of a hybrid bed at Le Marc. **D)** Pinch-out amalgamation zone at

Col du Fa. Debritic (Db) and turbiditc (Tb) sections can be identified and correlate with thick- and medium-bedded turbidites up-dip. It is difficult to differentiate groups of event-beds within these slope proximal units. **E)** Highly tractionally re-worked LDT. **F)** Typical thin-bedded LDT facies. **G)** Slumped thin-bedded turbidites at Argenton. Fold hinges indicate failure perpendicular to the slope.

Fig. 11: A) Contact between the thin-beds and higher-density turbidites at Col du Fa. The higher-density turbidites onlap against the low-density turbidite slope drape at an almost perpendicular incidence angle to the slope (arrow is paleoflow). **B)** Example of a high-density turbidite with a wedged base onlapping the underlying slope drape. Restoring the bed top to horizontal allows a rough estimate of the paleo-slope angle. **C)** Scar fill at Tête de Ruch (upper). The higher-density flows either onlap the scar drape abruptly or transform to low-density turbidites up the counter-slope. **D)** Laterally continuous hybrid-beds at Le Marc. These beds are interpreted to have been deposited away from the basin margin and cohesively transformed through distal run-out. 7 cm camera lens (black circle) for scale.

Fig. 12: High resolution log of one MDT approaching onlap at Col du Fa showing the short length-scale variability seen within these beds.

Fig. 13: Example of correlated low-density turbidites approaching the Col du Fa basin margin. Very little facies variation is seen within these beds.

Fig. 14: A) Hybrid bed evolution approaching topography at Argenton. **B)** Hybrid evolution at Tête de Ruch (lower**) C)** Hybrid bed evolution at the Tête de Ruch (upper). The complex interaction between the debritic and turbiditic intervals are suggested to result from either differential interaction with the slope between rheologically-distinct flow phases or erosion at the onlap surface. Letters in blacked boxes = correlated bed label.

Fig. 15: Outcrop sketch from the Col du Fa locality. **A)** Low-density turbidites drape the slope and are onlapped by higher-density turbidites. **B)** Flow transformation can be seen to occur in the proximal fringe deposits over 10-15 m approaching the onlap surface to the NW resulting in complex amalgamation zones at pinch out (see Fig. 10D for pinch-out detail).

Fig. 16: Summary logs showing facies transition approaching pinch-out toward basin margins for given lobe sub--environments and their dominant facies. The right hand petrographic images are taken from representative beds in the Annot Basin approaching onlap. The corresponding letter (white text in black box) on the logs indicates the point in the bed where the sample was taken.

Fig. 17: Synthesis of facies evolutions within the Grès d'Annot towards the basin margins and their stratigraphic position. Flow concentration at point of onlap dominantly controls the style of onlap termination. Lobe sub-environments are often obscured by flow-topography interaction, but can be 'back-stripped'.

Fig. 18: A) Run-up height versus flow sediment concentration. Flows with high concentrations are less able to run up topography than low-concentration flows. **B)** Run-up height versus the angle of incidence between the flow and the slope. Lower angles of incidence cause higher run-up of flows. **C)** Schematic diagram showing the relationship between frontal and lateral onlap (modified from Al A'Jaidi et al. 2004).

Fig. 19: Model for the stratigraphic evolution of flow terminations in a static confined deep-water basin. It is suggested that the pattern of termination trends may be used to predict the termination style expected at a given point on the onlap surface. Flow transformation results in highly concentrated flows, resulting in offlap. Similarly, bypass of the upper parts of axial flows results in offlap of the highly-concentrated basal layers of these flows against the underlying deposits. Concurrent hemipelagic deposition has been ignored for simplicity.

Fig. 20: Model for the progradation of a clastic system into an intra-slope minibasin. Representative logs (A, B and C) of the various sub-environments are indicated.

Fig. 21: Types of intra-formational onlap that may be recognised in confined deep-water basins (modified from Sinclair and Tomasso, 2002)**.** A distinction is made between autogenic onlap, caused by longitudinal flow evolution over shorter timescales, and allogenic onlap, caused by tectonic subsidence over longer timescales. Autogenic processes will create short-length scale heterogeneities within larger-scale and allogenically-driven sequences.

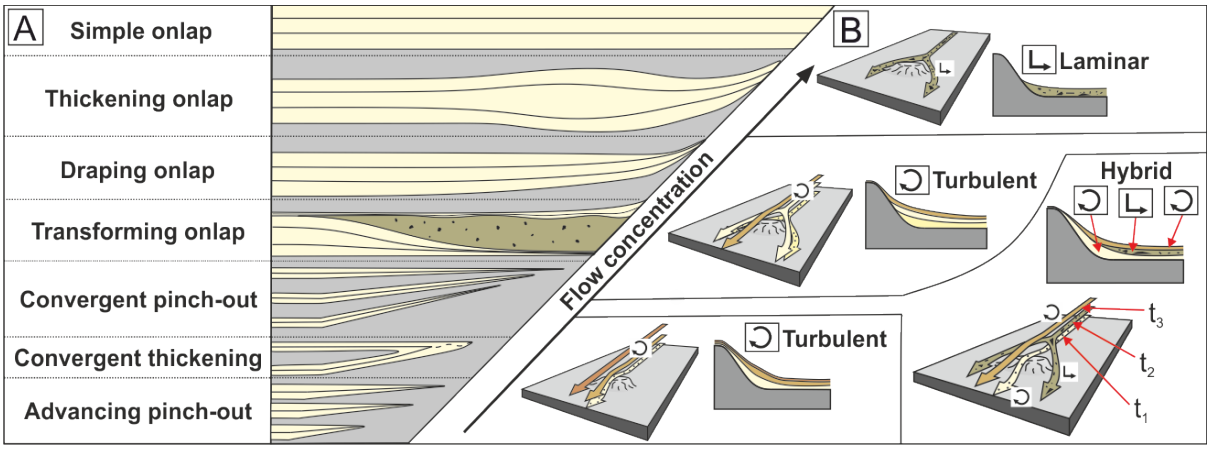
A
Simple onlap
Thickening onlap
Draping onlap
Transforming onlap
Convergent pinch-out
Convergent thickening
Advancing pinch-out
Flow concentration
B
Laminar
Turbulent
Hybrid
Turbulent
t3
t2
t1

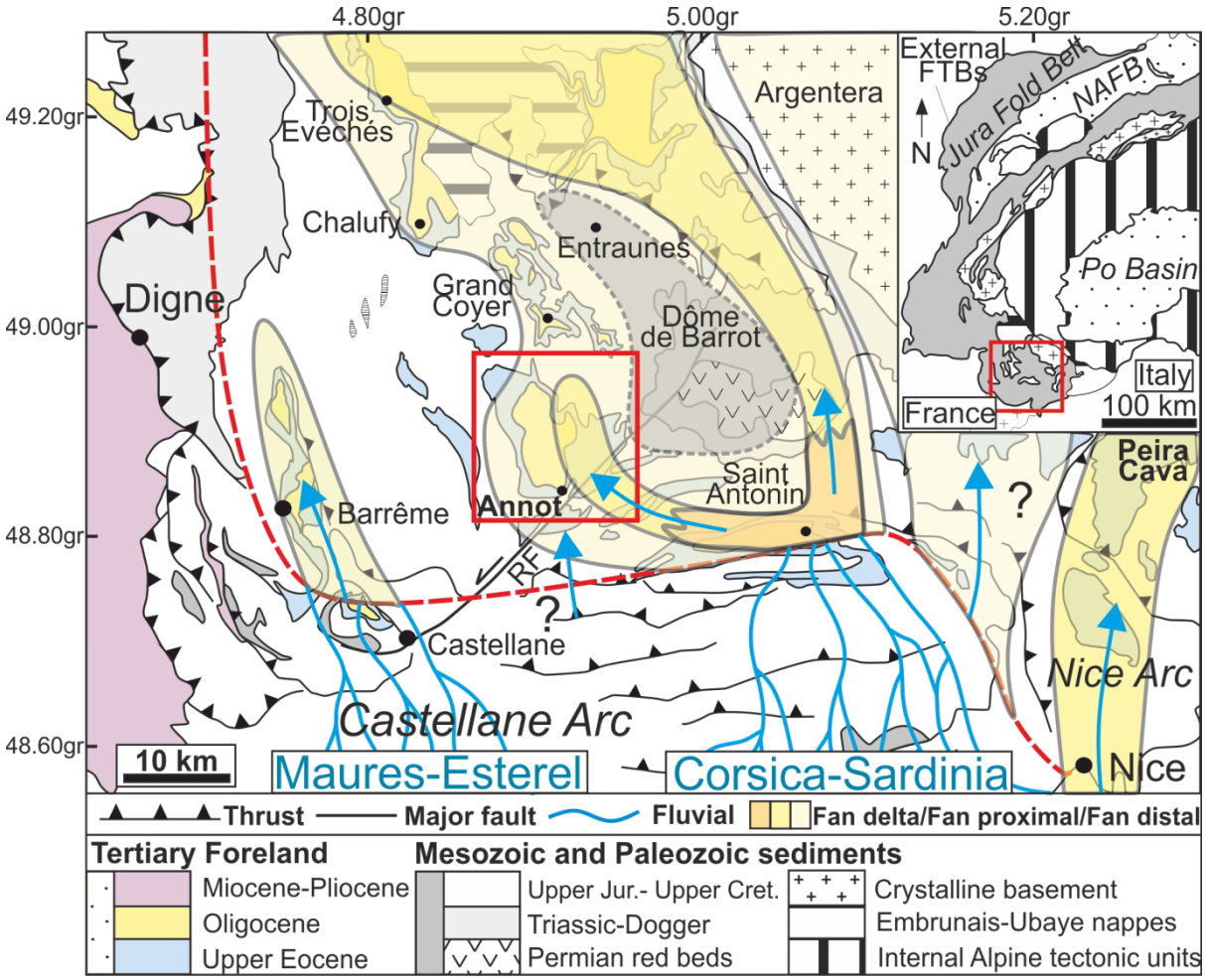
4.80gr
5.00gr
5.20gr
49.20gr
49.00gr
48.80gr
48.60gr
Trois Evêchés
Chalufy
Entraunes
Argentera
Grand Coyer
Dôme de Barrot
Digne
Barrême
Annot
Saint Antonin
RF
?
Castellane
Castellane Arc
10 km
Maures-Esterel
Corsica-Sardinia
Peira Cava
Nice Arc
Nice
External FTBs
N
Jura Fold Belt
NAFB
Po Basin
Italy
France
100 km
Thrust
Major fault
Fluvial
Fan delta/Fan proximal/Fan distal
Tertiary Foreland
Miocene-Pliocene
Oligocene
Upper Eocene
Mesozoic and Paleozoic sediments
Upper Jur.- Upper Cret.
Triassic-Dogger
Permian red beds
Crystalline basement
Embrunais-Ubaye nappes
Internal Alpine tectonic units

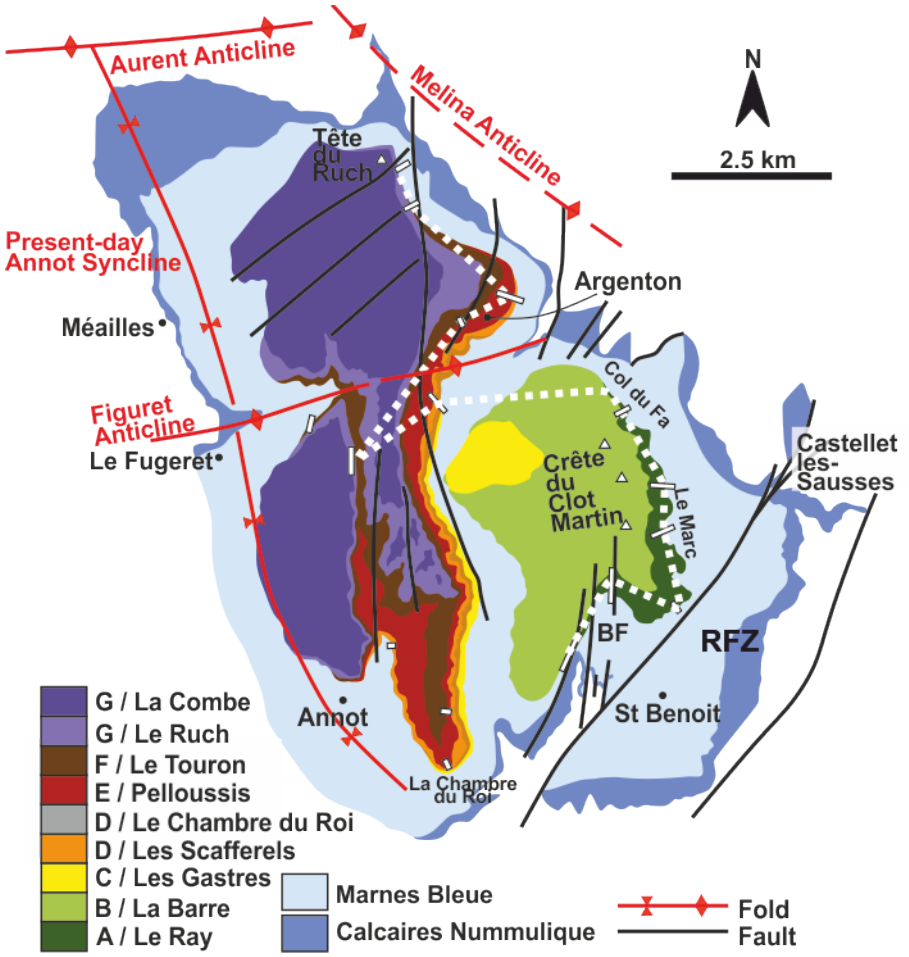
Aurent Anticline
Melina Anticline
N
2.5 km
Tête du Ruch
Present-day Annot Syncline
Argenton
Méailles
Col du Fa
Figuret Anticline
Le Fugeret
Crête du Clot Martin
Le Marc
Castellet les-Sausses
BF
RFZ
Annot
St Benoit
La Chambre du Roi
G / La Combe
G / Le Ruch
F / Le Touron
E / Pelloussis
D / Le Chambre du Roi
D / Les Scafferels
C / Les Gastres
B / La Barre
A / Le Ray
Marnes Bleue
Calcaires Nummulique
Fold
Fault

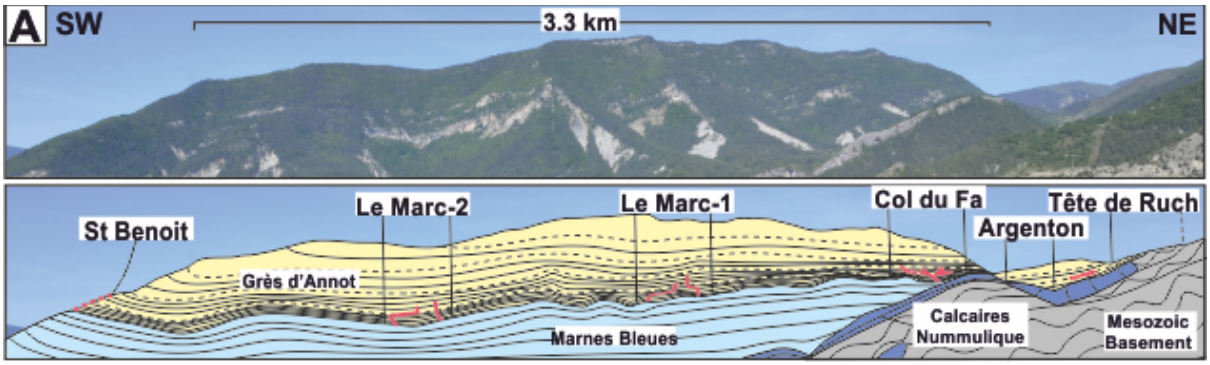
A
SW
3.3 km
NE
St Benoit
Le Marc-2
Le Marc-1
Col du Fa
Tête de Ruch
Argenton
Grès d'Annot
Marnes Bleues
Calcaires Nummulique
Mesozoic Basement


B
NE
SW
200 m

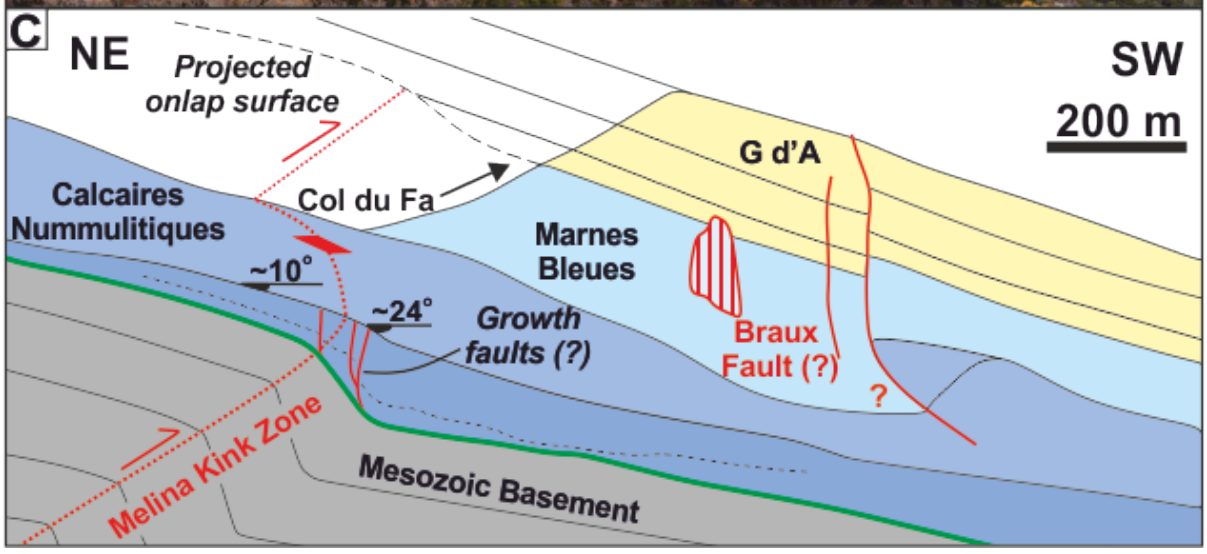
C
NE
SW
200 m
Projected onlap surface
Col du Fa
G d'A
Calcaires Nummulitiques
Marnes Bleues
~10°
~24°
Growth faults (?)
Braux Fault (?)
?
Melina Kink Zone
Mesozoic Basement

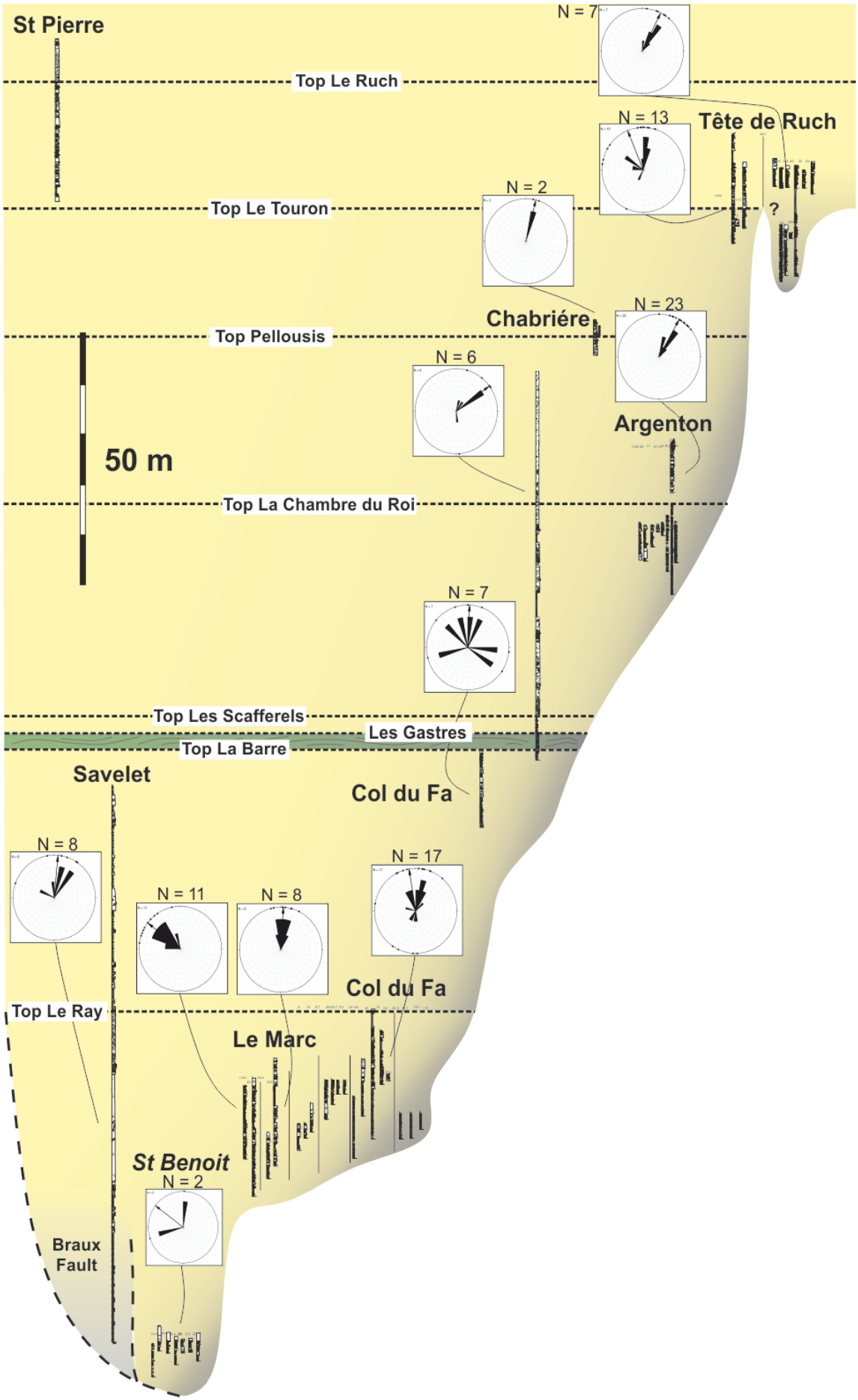
St Pierre
N = 7
Top Le Ruch
N = 13
Tête de Ruch
N = 2
Top Le Touron
?
Chabriére
N = 23
Top Pellousis
N = 6
Argenton
50 m
Top La Chambre du Roi
N = 7
Top Les Scafferels
Les Gastres
Top La Barre
Savelet
Col du Fa
N = 8
N = 17
N = 11
N = 8
Col du Fa
Top Le Ray
Le Marc
St Benoit
N = 2
Braux
Fault

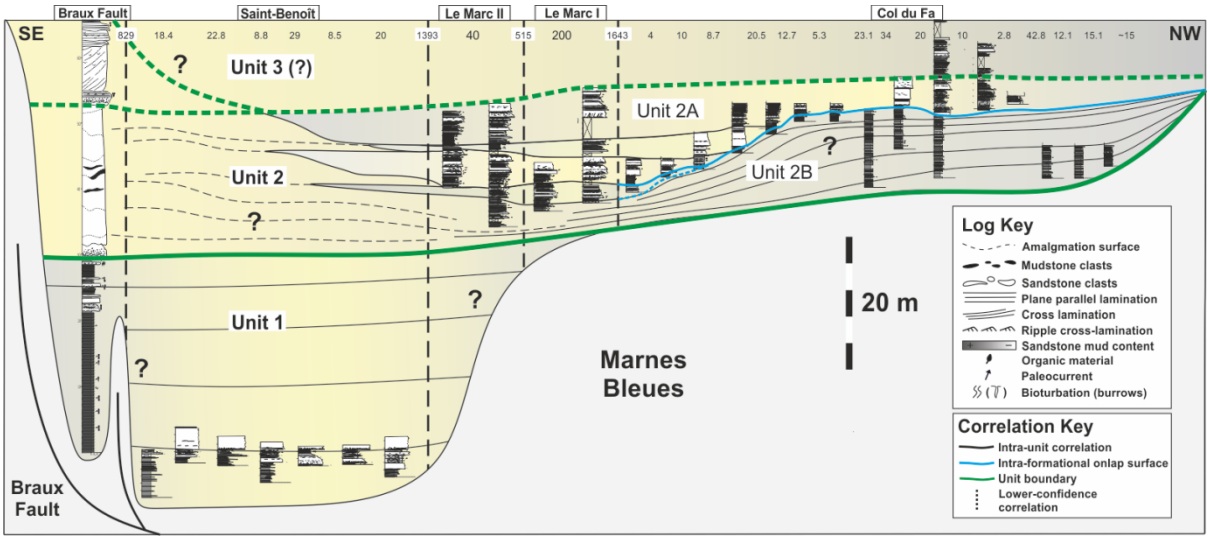
Braux Fault
Saint-Benoît
Le Marc II
Le Marc I
Col du Fa
SE
NW
829
18.4
22.8
8.8
29
8.5
20
1393
40
515
200
1643
4
10
8.7
20.5
12.7
5.3
23.1
34
20
10
2.8
42.8
12.1
15.1
~15
Unit 3 (?)
Unit 2A
Unit 2B
Unit 2
Unit 1
Marnes
Bleues
20 m
Braux
Fault
Log Key
Amalgmation surface
Mudstone clasts
Sandstone clasts
Plane parallel lamination
Cross lamination
Ripple cross-lamination
Sandstone mud content
Organic material
Paleocurrent
Bioturbation (burrows)
Correlation Key
Intra-unit correlation
Intra-formational onlap surface
Unit boundary
Lower-confidence
correlation

Lithofacies	Description	Interpretation	Facies Association	Onlap Geometry
Thick-bedded sandstone (LF 1)	Forms 1 - 20 m amalgamated packages or 0.5 - 2 m beds, Medium - granule grain size. Flat or weakly erosive bed bases and flat bed tops. Mostly structreless with some planar laminations. Often contains mud clasts (<5 cm) and soft sediment deformation e.g. flames and dishes.	Rapid aggradation beneath a highly concentrated flow. Planar-spaced laminae indicate traction carpet deposition *(sensu* Lowe, 1982).	Lobe axis (FA 1) Lobe off-axis	Abrupt termination High-density flows deposit abruptly at counter-slope due to loss of capacity, compared to lower concentration flows with otherwise similar flow properties (e.g. Hiscott, 1994). The slope may be draped by deposition from the overriding and dilute tail of the same flow (e.g., Li et al., 2017).
Medium-bedded sandstone (LF 2)	0.1 - 0.8 m beds. Fine - coarse grain size. Flat or weakly erosive bed bases and flat or convolute bed tops. Flutes and grooves on bed bases. Sporadic granules sometimes present and associated with structureless lower bed divisions. Mostly normally graded with planar and convolute laminations. Ripples at bed tops.	Presence of flutes, normal grading and tractional structures indicates deposition from a dilute turbidity current. These beds are interpreted as medium-density turbidites due to their often structureless basal divisions and thicknesses greater than 10 cm.	Lobe off-axis (FA 2) Lobe axis Proximal fringe	Abrupt to draped termination More capable of surmounting topography than higher-density flows because they are more able to maintain turbulent energy while flowing up the counter-slope (e.g. Bakke et al., 2013; Eggenhuisen et al. 2017). Wide variety of sediment concentrations in these flows causes drape to extend from metres to tens of metres up the slope.
Hybrid beds (LF 3)	0.1 - 1.2 m bi- or tri-partite beds. Lower medium-coarse sandstones (division 1) overlain sharply or loaded by argillaceous sandstones (division 2). Argillaceous sandstones often have a sheared fabric. Cleaner, often finer, and tractionally reworked sandstone sometimes present capping these divisions with a sharp or foundered base (division 3). Decimetre scale organic material sometimes present in middle division.	Beds containing deposits of both turbulent and transitional/ laminar flows interpreted as hybrid beds *(sensu* Haughon et al. 2009). Flow transformation occurs through increasing concentration of fines during run-out (e.g. Kane et al. 2017) or through forced deceleration (Barker et al. 2008; Patacci et al. 2014).	Proximal fringe (FA 3) Lobe off-axis Distal fringe Lobe axis	Abrupt to draped termination Debritic or argillaceous middle divisions are highly concentrated so terminate abruptly. Draping of the middle division may occur if the slope is shallow enough to allow run-up of the debritic middle division. The turbulent lower part of the flow may drape the slope and amalgamate with the overlying sandstone or deposit abruptly if high-density.
Thin-bedded sandstone (LF 4)	0.01 - 0.1 m siltstones and fine sandstones. Parallel and convolute laminations, normal grading. Flutes rarely preserved. Ripples occasionally show opposing paleoflow directions.	Fine grain size, thin event beds and abundance of tractional structures indicates that these beds were deposited by low-density/concentration turbidity current and are therefore interpreted as low-density turbidites.	Distal fringe (FA 4) Proximal fringe Lobe off-axis	Draped termination Low concentration flows are less affected by changes in slope angle and are thus able to surmount basin topography and drape topography for substantial distances up the counter-slope (e.g. Muck and Underwood, 1990). Low-density turbidites are therefore able dominate much of the sediment thickness on the upper parts of the confining slope.

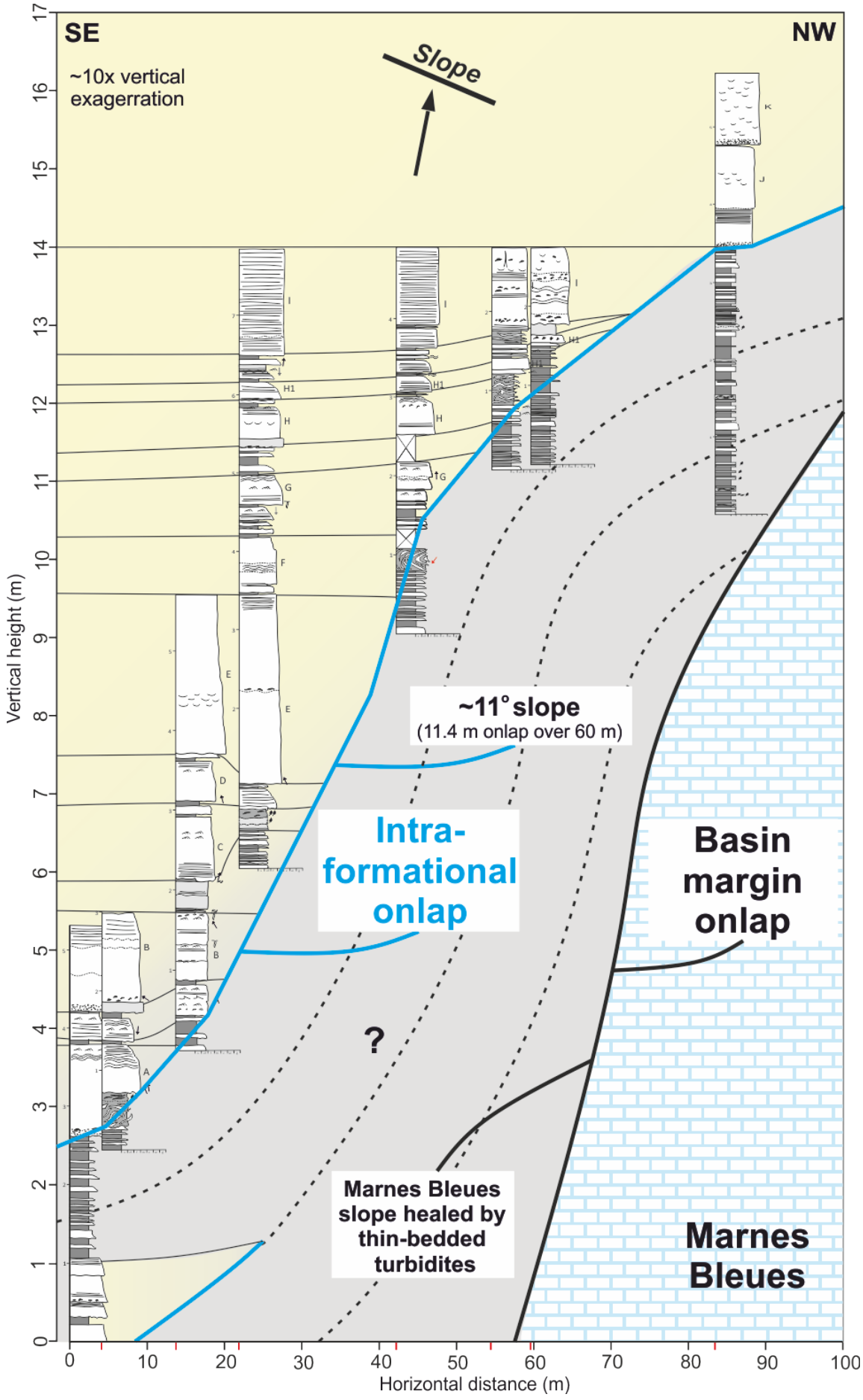
SE
NW
~10x vertical exagerration
Slope
~11° slope
(11.4 m onlap over 60 m)
Intra-formational onlap
Basin margin onlap
?
Marnes Bleues slope healed by thin-bedded turbidites
Marnes Bleues
Vertical height (m)
Horizontal distance (m)
0
10
20
30
40
50
60
70
80
90
100
1
2
3
4
5
6
7
8
9
10
11
12
13
14
15
16
17

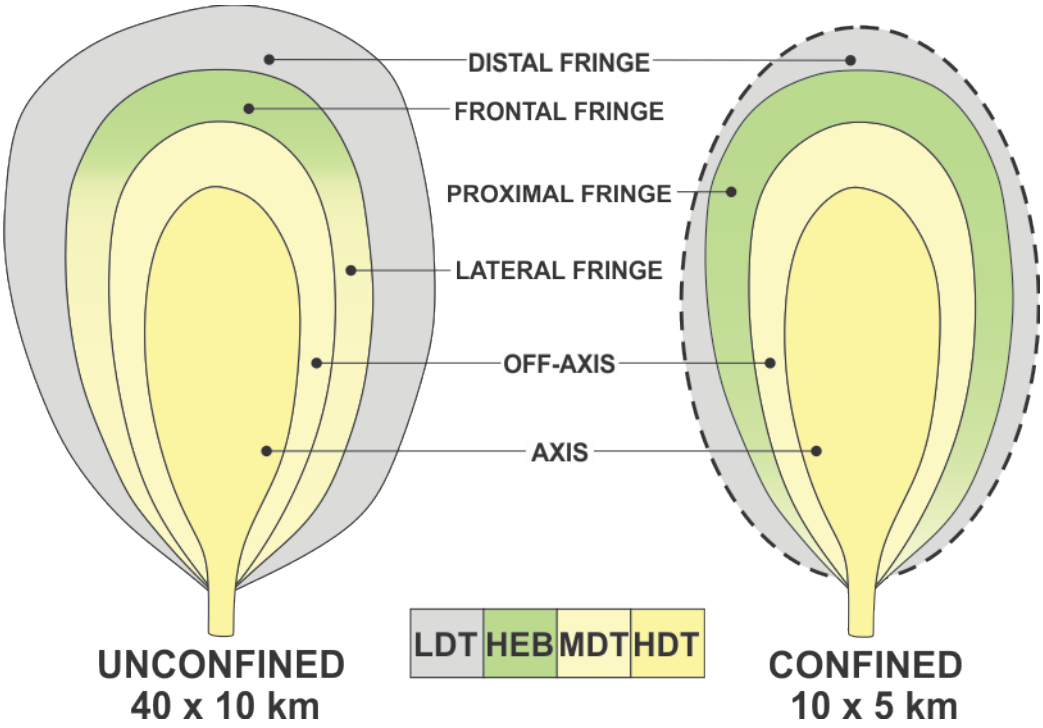
DISTAL FRINGE
FRONTAL FRINGE
PROXIMAL FRINGE
LATERAL FRINGE
OFF-AXIS
AXIS
LDT
HEB
MDT
HDT
UNCONFINED
40 x 10 km
CONFINED
10 x 5 km

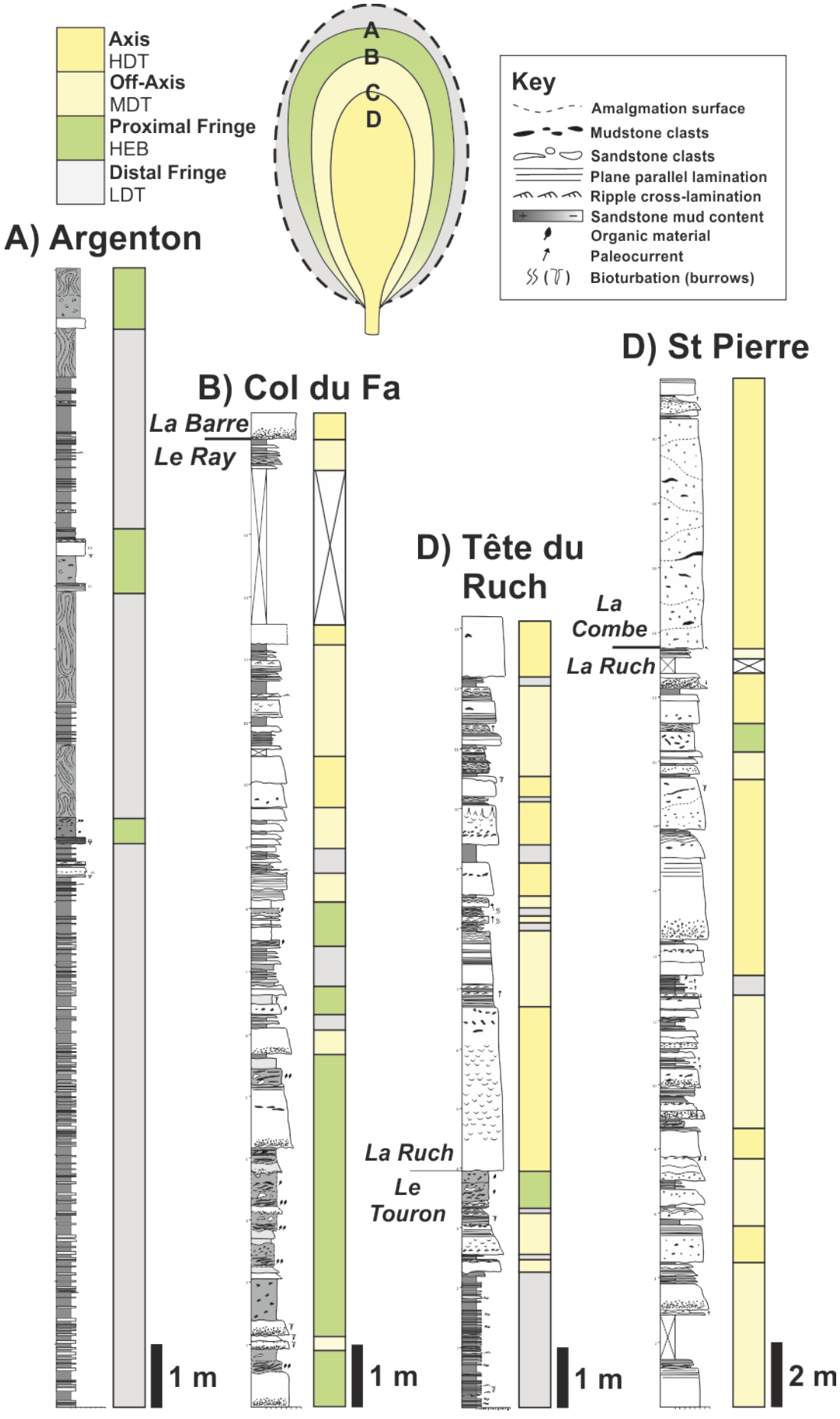
Axis
HDT
Off-Axis
MDT
Proximal Fringe
HEB
Distal Fringe
LDT
A
B
C
D
Key
Amalgmation surface
Mudstone clasts
Sandstone clasts
Plane parallel lamination
Ripple cross-lamination
Sandstone mud content
Organic material
Paleocurrent
Bioturbation (burrows)
A) Argenton
B) Col du Fa
La Barre
Le Ray
D) Tête du Ruch
La Ruch
Le Touron
D) St Pierre
La Combe
La Ruch
1 m
1 m
1 m
2 m

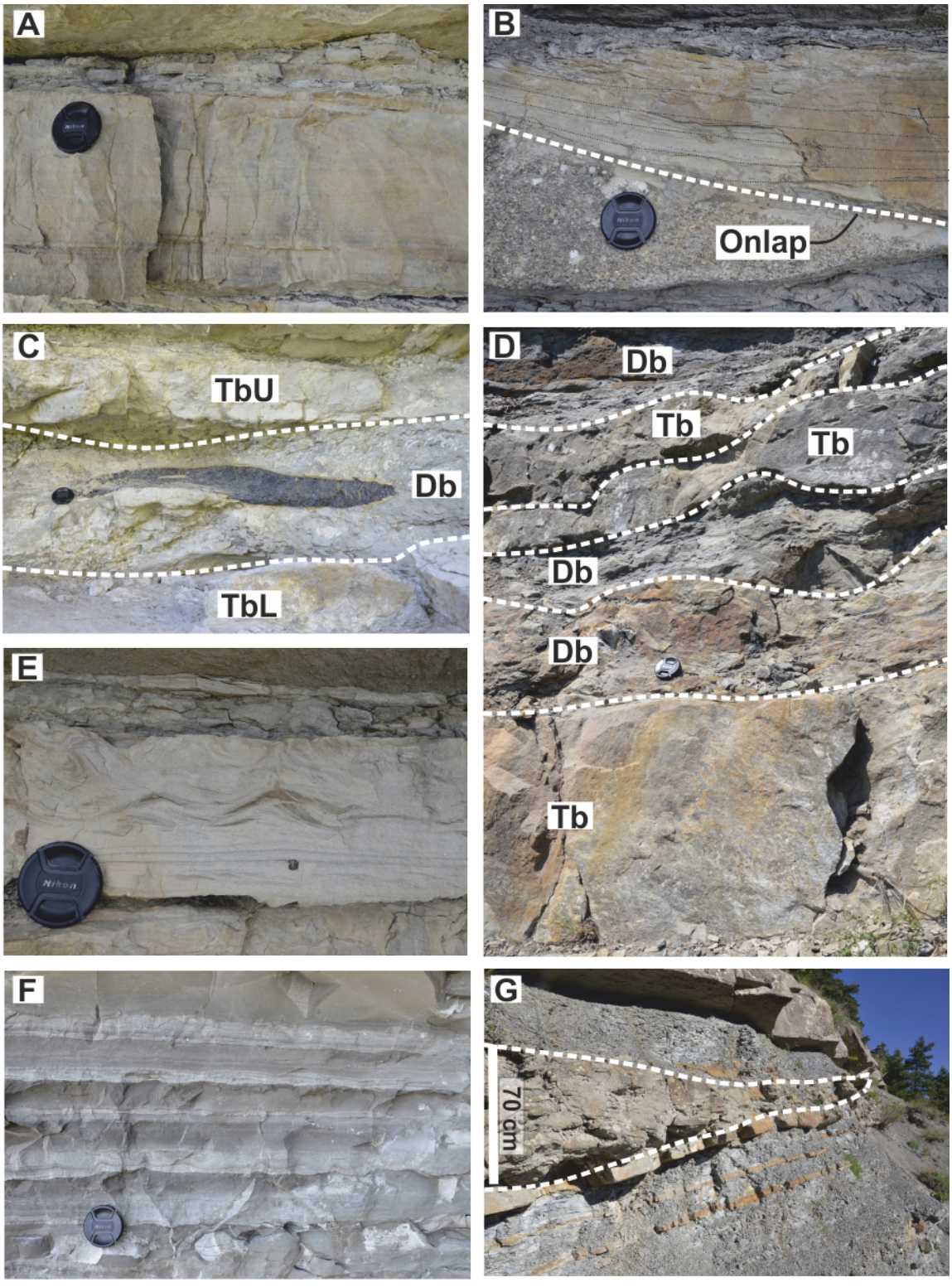
A
B
Onlap
C
TbU
Db
TbL
D
Db
Tb
Tb
Db
Db
Tb
E
F
G
70 cm

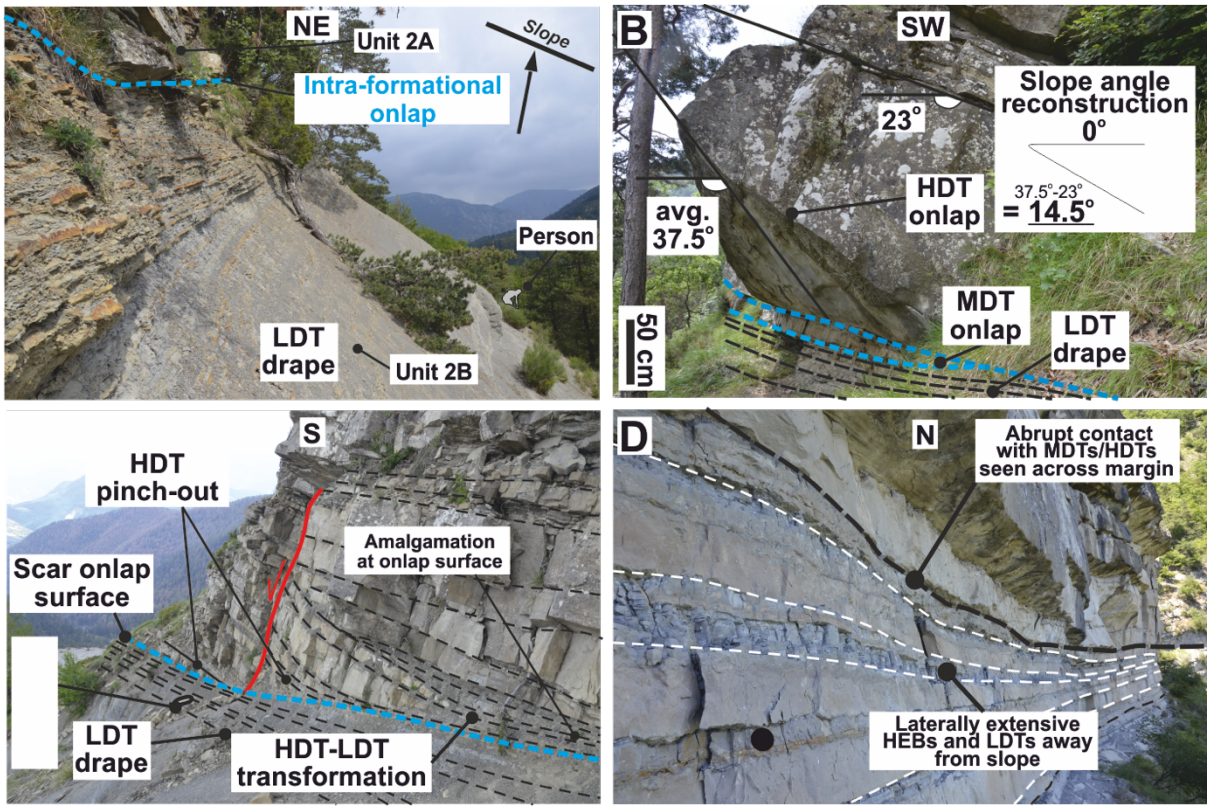
NE
Unit 2A
Slope
Intra-formational onlap
Person
LDT drape
Unit 2B
B
SW
Slope angle reconstruction
0°
23°
HDT onlap
37.5°-23°
= 14.5°
avg. 37.5°
50 cm
MDT onlap
LDT drape
S
HDT pinch-out
Amalgamation at onlap surface
Scar onlap surface
LDT drape
HDT-LDT transformation
D
N
Abrupt contact with MDTs/HDTs seen across margin
Laterally extensive HEBs and LDTs away from slope

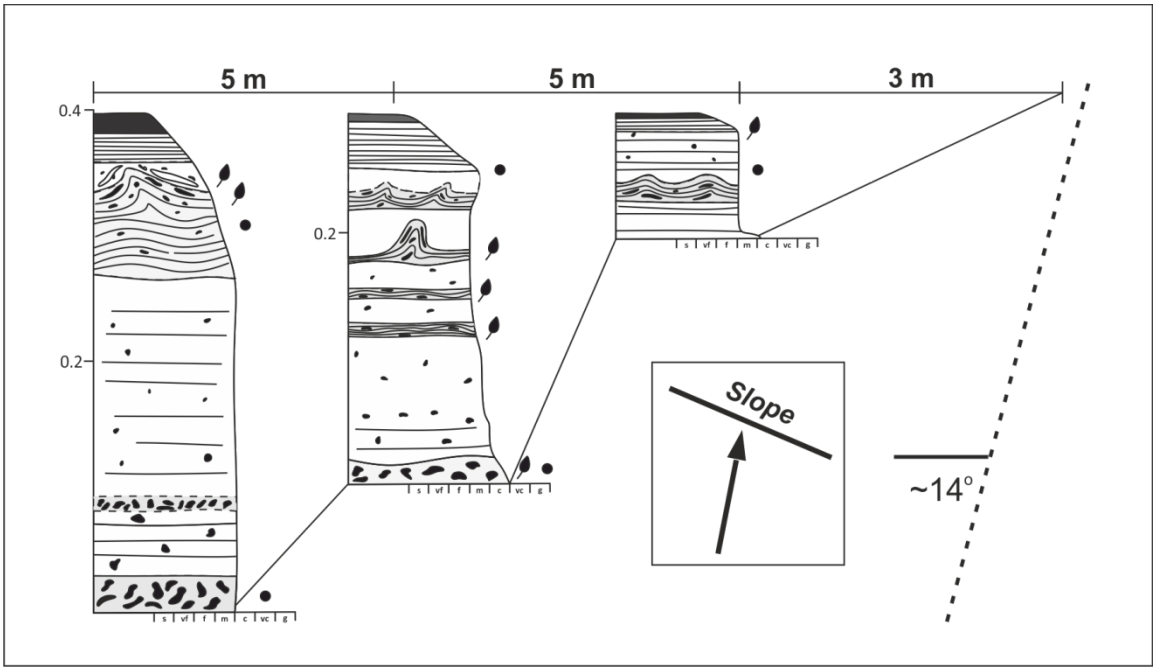
5 m
5 m
3 m
0.4
0.2
0.2
s vf f m c vc g
s vf f m c vc g
s vf f m c vc g
Slope
~14°

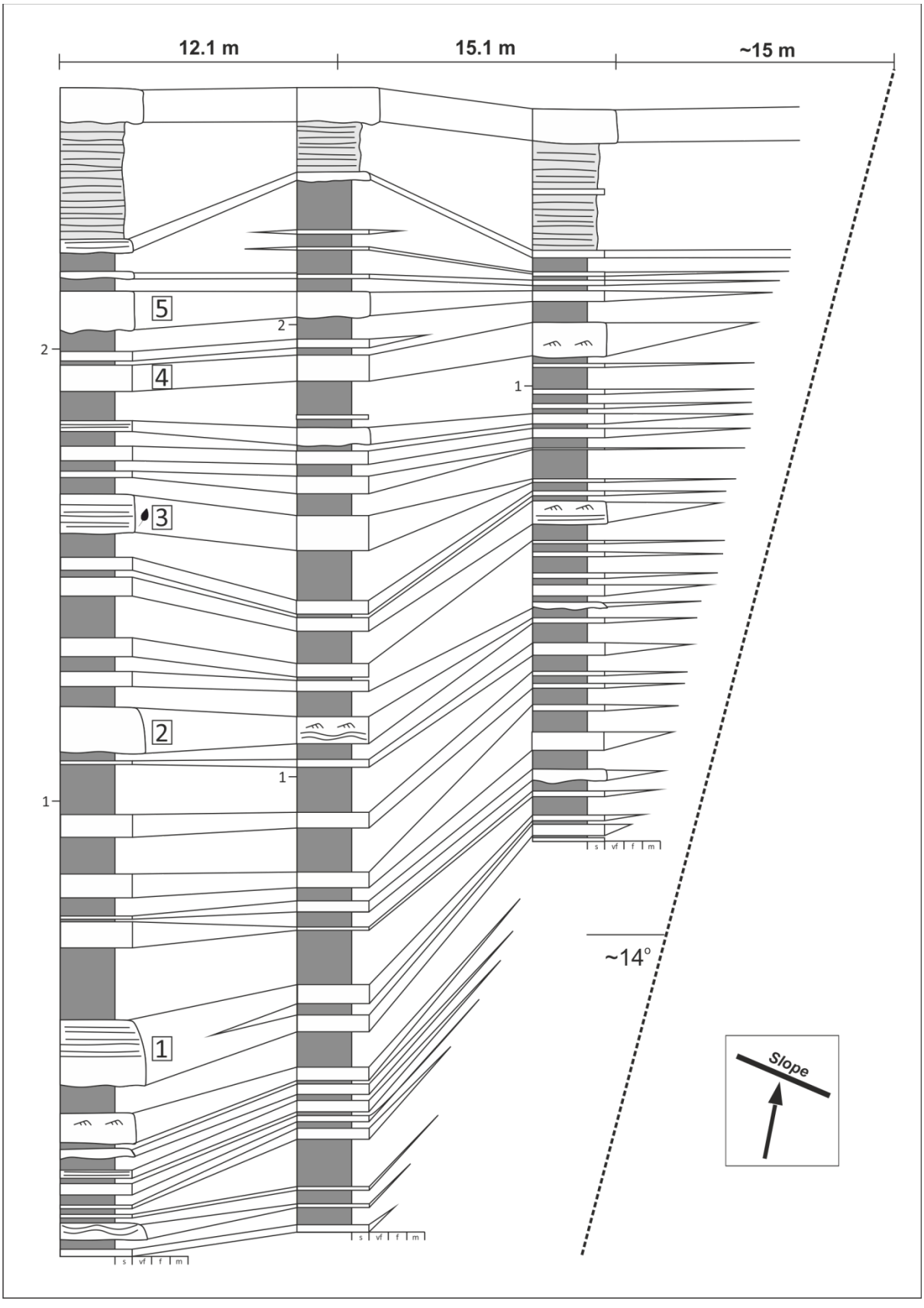
12.1 m
15.1 m
~15 m
5
4
3
2
1
2
1
2
1
s vf f m
s vf f m
s vf f m
~14°
Slope

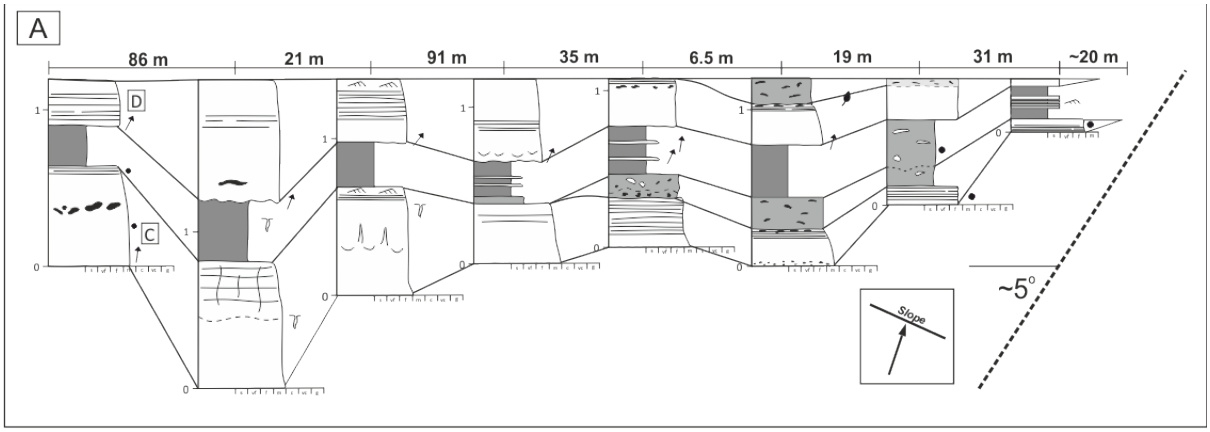
A
86 m
21 m
91 m
35 m
6.5 m
19 m
31 m
~20 m
D
C
~5°
Slope

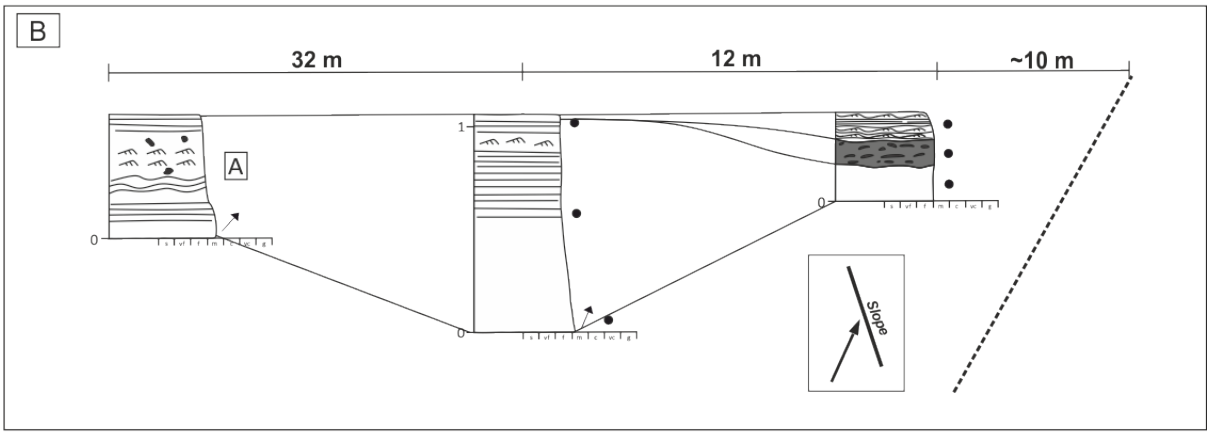
B
32 m
12 m
~10 m
A
Slope

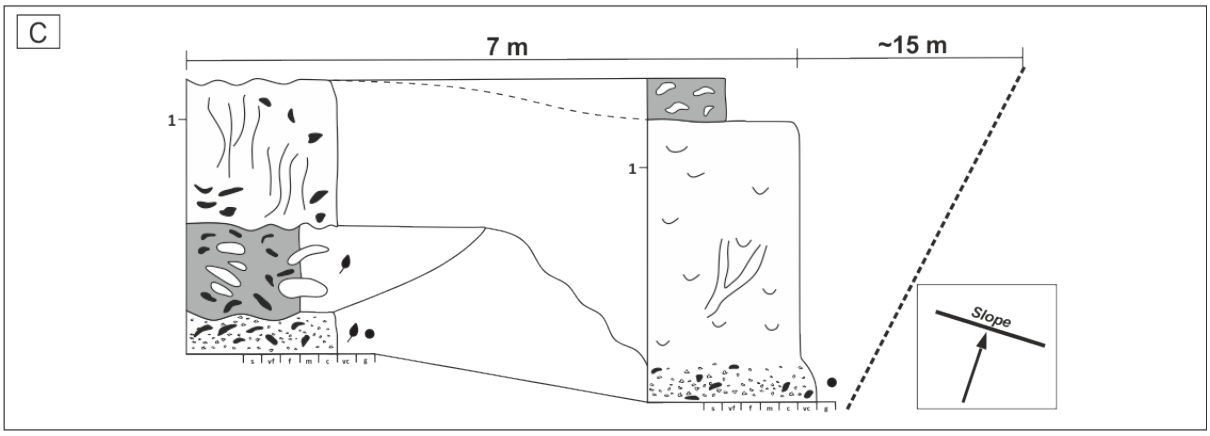
C
7 m
~15 m
Slope

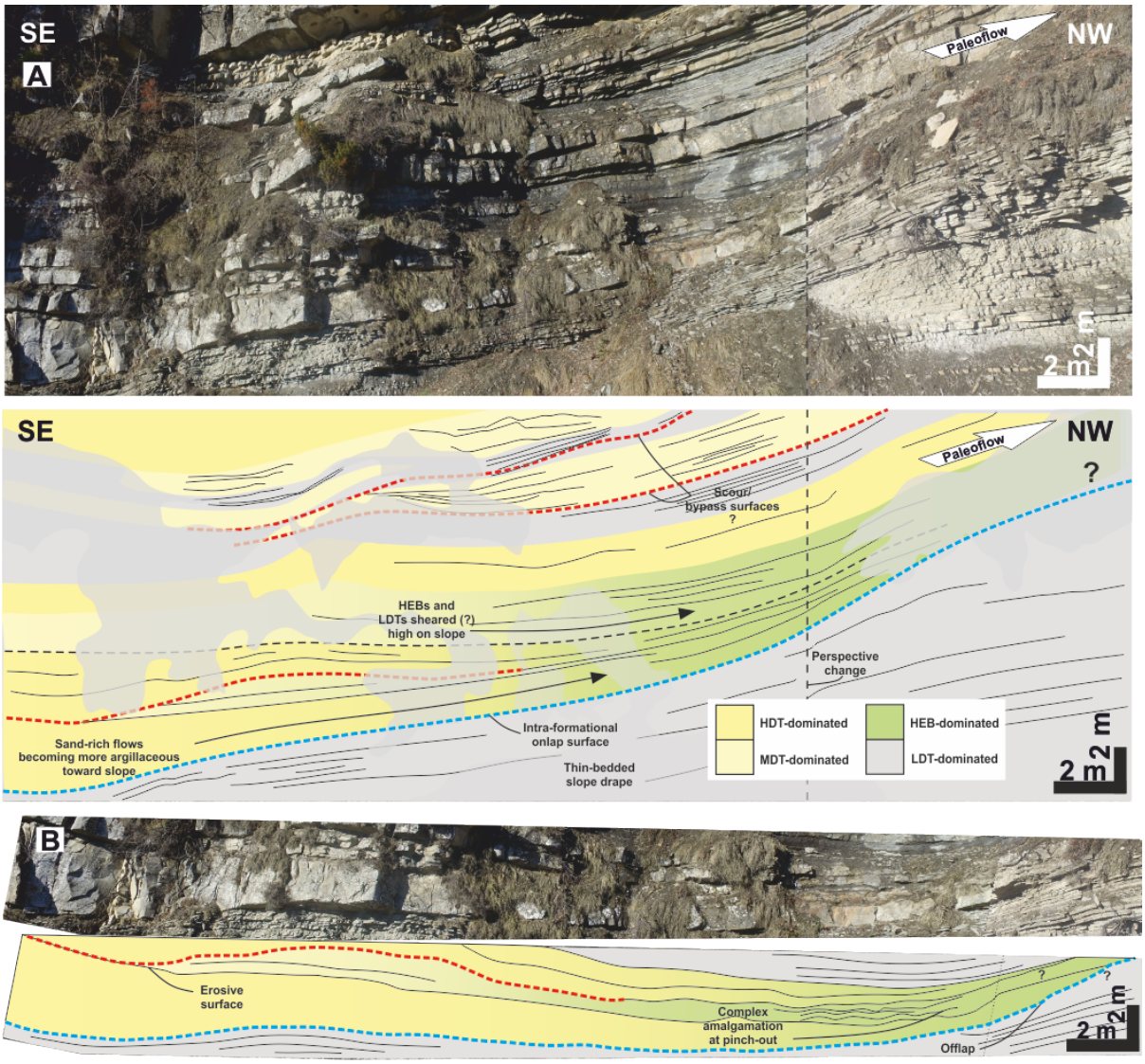
SE
A
Paleoflow
NW
2 m
SE
NW
Paleoflow
?
Scour/
bypass surfaces
?
HEBs and
LDTs sheared (?)
high on slope
Perspective
change
Intra-formational
onlap surface
Sand-rich flows
becoming more argillaceous
toward slope
Thin-bedded
slope drape
HDT-dominated
MDT-dominated
HEB-dominated
LDT-dominated
2 m
B
Erosive
surface
Complex
amalgamation
at pinch-out
Offlap
?
?
2 m

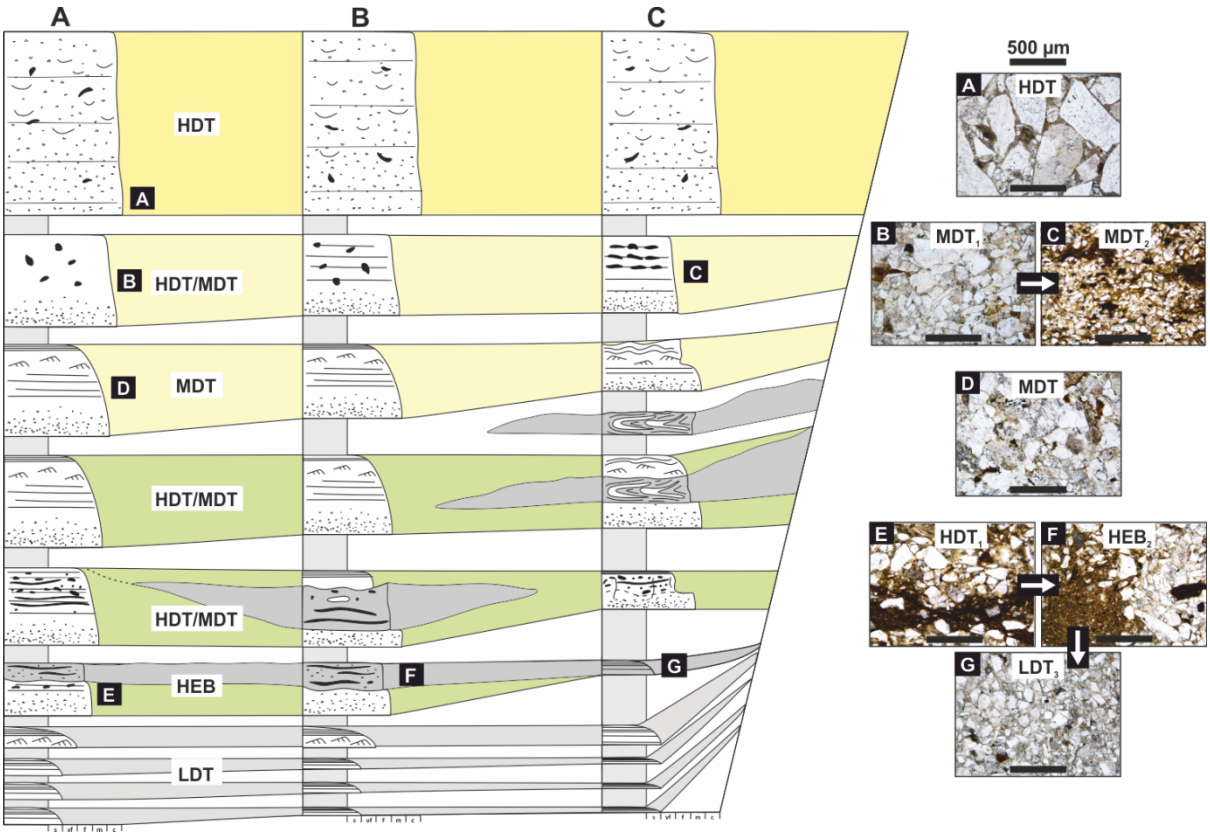
A
B
C
HDT
A
B
HDT/MDT
C
D
MDT
HDT/MDT
HDT/MDT
E
HEB
F
G
LDT
500 µm
A
HDT
B
MDT1
C
MDT2
D
MDT
E
HDT1
F
HEB2
G
LDT3

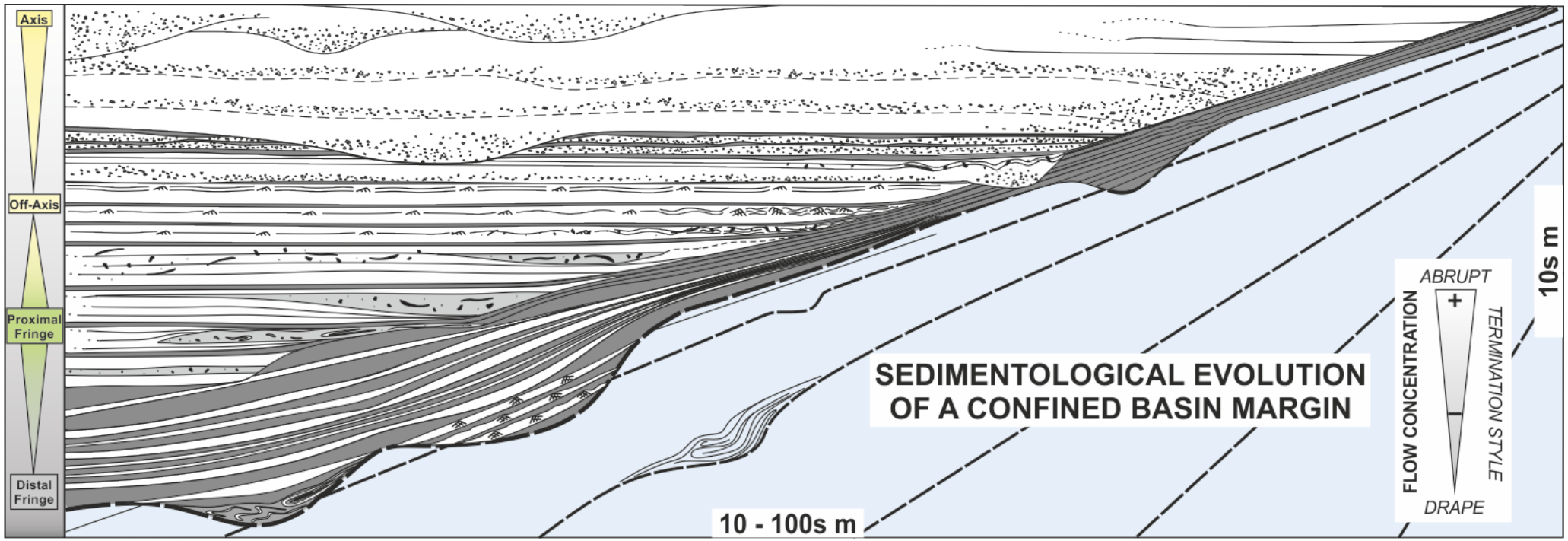
Axis
Off-Axis
Proximal Fringe
Distal Fringe
SEDIMENTOLOGICAL EVOLUTION
OF A CONFINED BASIN MARGIN
10 - 100s m
10s m
FLOW CONCENTRATION
ABRUPT
+
DRAPE
TERMINATION STYLE

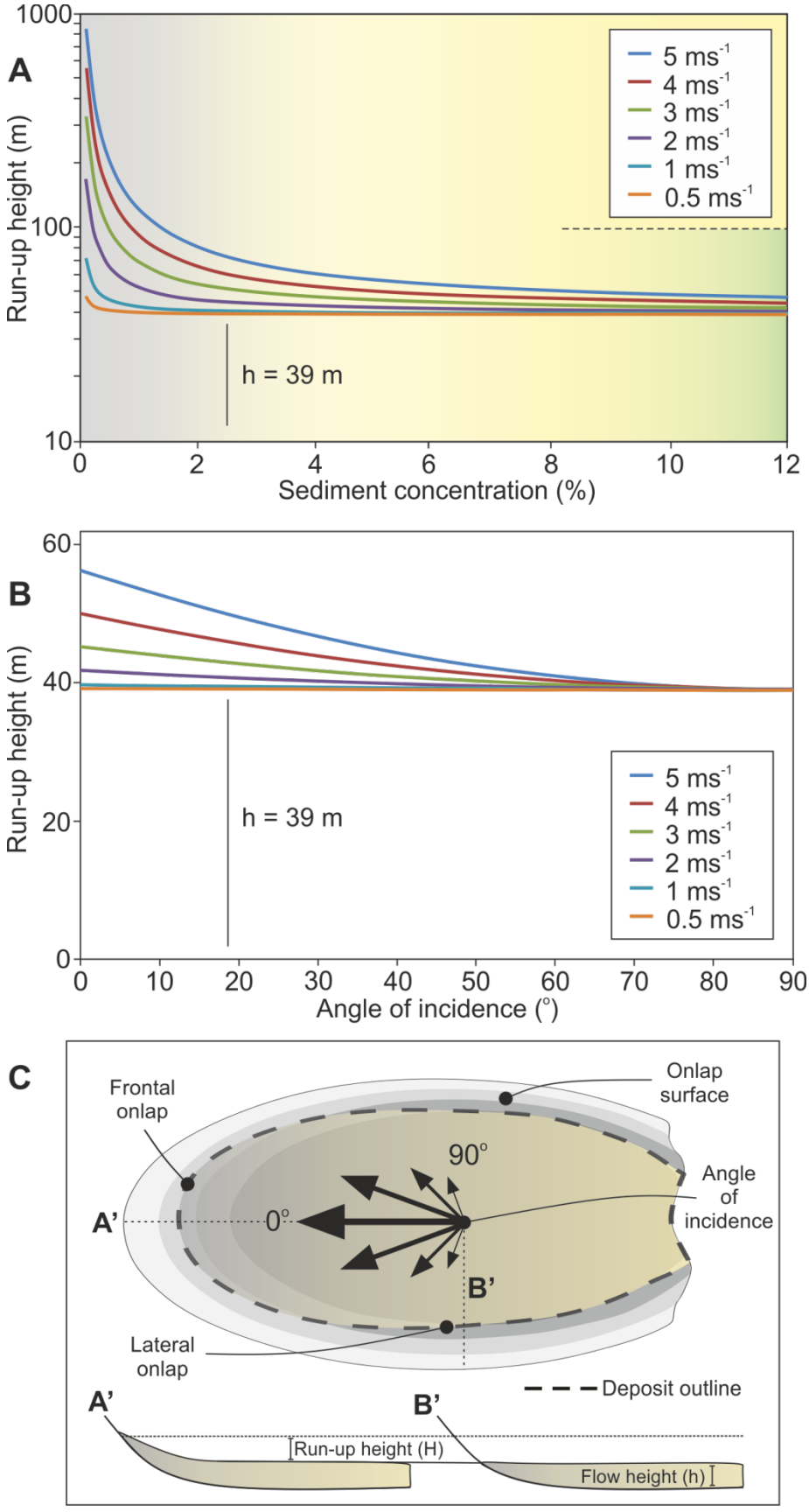
A
1000
100
10
Run-up height (m)
5 ms-1
4 ms-1
3 ms-1
2 ms-1
1 ms-1
0.5 ms-1
h = 39 m
0
2
4
6
8
10
12
Sediment concentration (%)
B
60
40
20
0
Run-up height (m)
h = 39 m
5 ms-1
4 ms-1
3 ms-1
2 ms-1
1 ms-1
0.5 ms-1
0
10
20
30
40
50
60
70
80
90
Angle of incidence (°)
C
Frontal onlap
Onlap surface
90°
Angle of incidence
A'
0°
B'
Lateral onlap
Deposit outline
A'
B'
Run-up height (H)
Flow height (h)

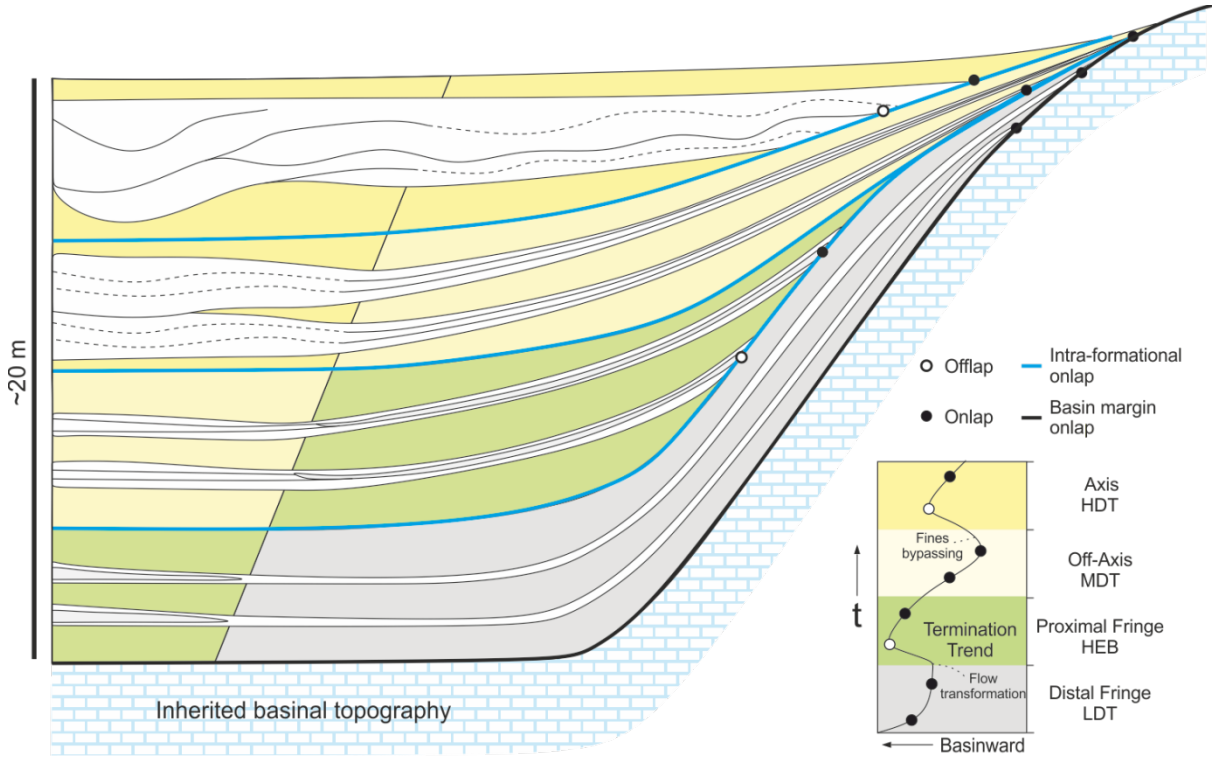
~20 m
Inherited basinal topography
Offlap
Onlap
Intra-formational onlap
Basin margin onlap
t
Fines bypassing
Termination Trend
Flow transformation
Axis HDT
Off-Axis MDT
Proximal Fringe HEB
Distal Fringe LDT
Basinward

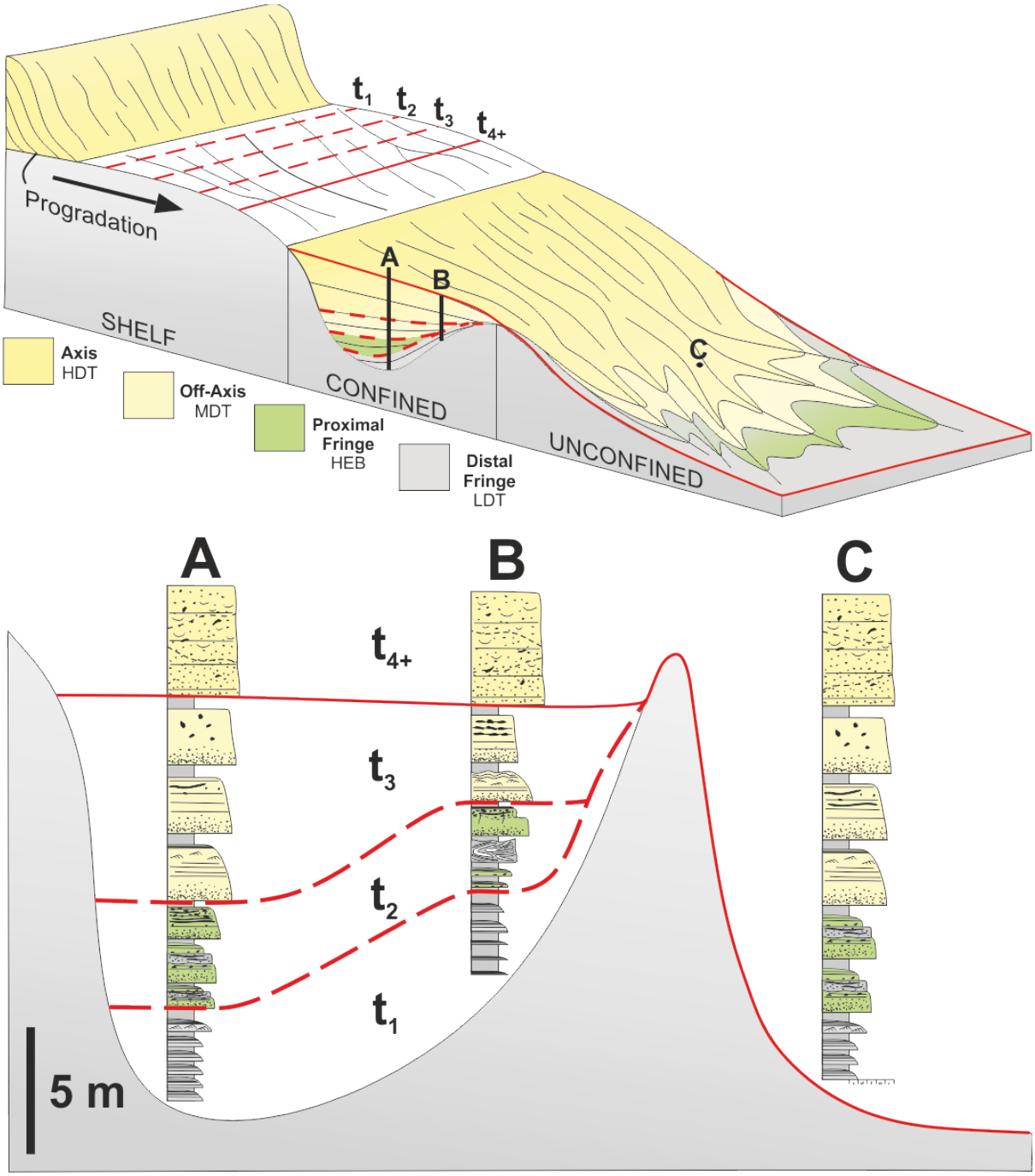
t1 t2 t3 t4+
Progradation
A
B
C
SHELF
CONFINED
UNCONFINED
Axis
HDT
Off-Axis
MDT
Proximal
Fringe
HEB
Distal
Fringe
LDT
A
B
C
t4+
t3
t2
t1
5 m

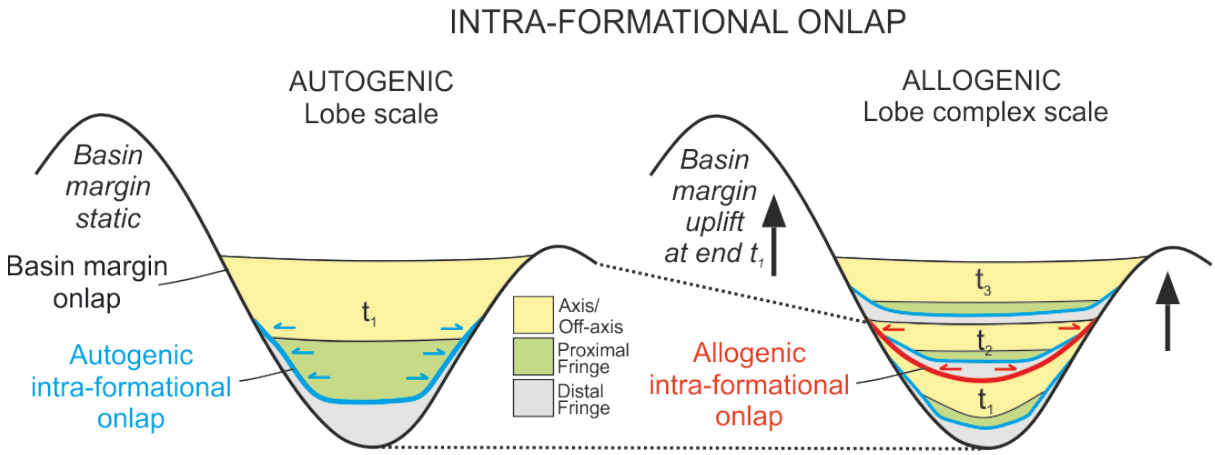
INTRA-FORMATIONAL ONLAP
AUTOGENIC
Lobe scale
ALLOGENIC
Lobe complex scale
Basin margin static
Basin margin onlap
Autogenic intra-formational onlap
t1
Axis/ Off-axis
Proximal Fringe
Distal Fringe
Basin margin uplift at end t1
Allogenic intra-formational onlap
t3
t2
t1